Journal of Magnetic Resonance 197 (2009) 193–207

Contents lists available at ScienceDirect

Journal of Magnetic Resonance

journal homepage: www.elsevier.com/locate/jmr

# Effects of *L*-spin longitudinal quadrupolar relaxation in *S*{*L*} heteronuclear recoupling and *S*-spin magic-angle spinning NMR

Y.-Y. Hu, K. Schmidt-Rohr *

*Ames Laboratory and Department of Chemistry, Iowa State University, Ames, IA 50011, USA*

ARTICLE INFO

*Article history:*
Received 12 November 2008
Revised 19 December 2008
Available online 13 January 2009

*Keywords:*
Heteronuclear recoupling
Quadrupolar relaxation
$T_2$ in solids
Self-decoupling
$^{14}$N

ABSTRACT

In experiments on *S*–*L* heteronuclear spin systems with evolution of the *S*-spin magnetization under the influence of a quadrupolar nucleus (*L*-spin), effects of longitudinal quadrupolar ($T_{1Q}$) relaxation of the *L*-spin coherence on the sub-millisecond time scale have been documented and explored, and methods for minimizing their effect have been demonstrated. The longitudinal relaxation results in heteronuclear dephasing even in the reference signal $S_0$ of *S*{*L*} REDOR, REAPDOR, RIDER, or SPIDER experiments, due to $T_{1Q}$-relaxation of the transiently generated $S_yL_z$ coherence, reducing or even eliminating the observable dephasing $\Delta S$. Pulse sequences for measuring an improved reference signal $S_{00}$ with minimal heteronuclear recoupling but the same number of pulses as for $S_0$ and *S* have been demonstrated. From the observed intensity $\Delta S_0 = S_{00} - S_0$ and the SPIDER signal $\Delta S/S_0$, $T_{1Q}$ can be estimated. Accelerated decays analogous to the dipolar $S_0$ curves will occur in $T_2$ measurements for *J*-coupled *S*–*L* spin pairs. Even in the absence of recoupling pulses, fast $T_{1Q}$ relaxation of the unobserved nucleus shortens the transverse relaxation time $T_{2S,MAS}$ of the observed nucleus, in particular at low spinning frequencies, due to unavoidable heteronuclear dipolar evolution during a rotation period. The observed spinning-frequency dependence of $T_{2S,MAS}$ matches the theoretical prediction and may be used to estimate $T_{1Q}$. The effects are demonstrated on several $^{13}$C{$^{14}$N} spin systems, including an arginine derivative, the natural *N*-acetylated polysaccharide chitin, and a model peptide, $(POG)_{10}$.



## 1. Introduction

Recoupling of heteronuclear dipolar interactions has proven extremely useful for structure determination [1,2]. While initially developed to probe the distance between two different isotopes with spin 1/2, it has also been extended to quadrupolar nuclei. The REAPDOR [3,4] and SPIDER [5] methods use pulse sequences with most 180° recoupling pulses applied to the observed spin-1/2 nucleus, see Fig. 1, but differ in the pulses applied in the center of the recoupling sequence to invert or saturate the spin state of the quadrupolar nucleus. Recently, closely related methods for two-dimensional correlation of $^{14}$N and $^{13}$C bands based on heteronuclear recoupling have also attracted significant attention [6,7].

In this paper, we discuss and demonstrate the effects of fast $T_{1Q}$ relaxation of the quadrupolar nucleus on the *S*{*L*} heteronuclear dephasing. Due to the large coupling-strength prefactors of the longitudinal relaxation rate, the $T_{1Q}$ relaxation times of quadrupolar nuclei can be short, less than 0.1 ms. In solution NMR, the very short $T_{1Q}$ results in "self-decoupling" of the *L*-spin from the *S*-spin [8–10]. In the solid state, it has usually been assumed implicitly that $T_{1Q}$ exceeds the recoupling time $Nt_r$, but we show several experimental examples, namely a molecular crystal (an arginine derivative), a 30-residue collagen-mimetic peptide, and the biopolymer chitin, where this does not hold. We demonstrate a pulse sequence that has the same number and type of pulses as the standard $S_0$ pulse sequence for recoupling involving heteronuclei with very broad spectra, but minimizes heteronuclear recoupling and thus the $T_{1Q}$-relaxing two-spin coherence. The difference $\Delta S_0$ between the resulting "$S_{00}$" signal and the standard $S_0$ signal is dominated by peaks that fail to show the expected dephasing in SPIDER, as a result of reduced $S_0$ intensity. In $^{14}$N–$^{13}$C correlation spectra, such $^{14}$N sites with $T_{1Q}$-relaxation on the 0.2-ms time scale would not produce any signal. We derive the differential equations for simultaneous heteronuclear coupling and relaxation, with analytical solutions for $L = 1/2$ and numerical calculations for $L = 1/2$, 1, and 3/2, that produce the expected decrease of the apparent $T_2$ of the observed *S*-spin under MAS ($T_{2S,MAS}$) in $S_0$ measurements for $T_{1Q} \approx 1$ ms, as well as the increase of $T_{2S,\,MAS}$ and loss of heteronuclear evolution for very short $T_{1Q}$, i.e. self-decoupling of the quadrupolar nucleus.

Due to transient coupling effects during MAS, $T_{1Q}$ relaxation of the quadrupolar heteronucleus also results in homogeneous line-broadening of the observed signal without any recoupling.

* Corresponding author.
*E-mail address:* srohr@iastate.edu (K. Schmidt-Rohr).

1090-7807/$ - see front matter © 2009 Elsevier Inc. All rights reserved.
doi:10.1016/j.jmr.2008.12.021

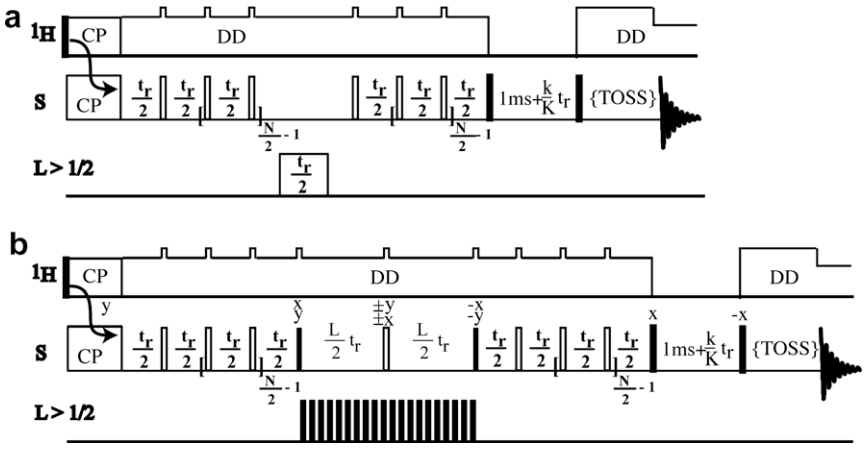


**Fig. 1.** Pulse sequences for (a) $S\{L\}$ REAPDOR and (b) $S\{L\}$ SPIDER with $L > 1/2$. Pulses with 90° flip angles are shown as narrow filled rectangles, 180° pulses as narrow unfilled rectangles. The irradiation on the $L$-spin in SPIDER consists of closely spaced ~2-μs pulses with ~1-μs spacing. Reference signals $S_0$ are obtained without irradiation on the $L$-spin, but with the train of 180° pulses on $S$.

The expected and observed increase in $T_{2S,MAS}$ with spinning-frequency $\omega_r$ matches well with the simulations, which provides an estimate of $^{14}N$ $T_1$. Finally, we also explore the origin of the enhanced $^{14}N$ $T_1$ relaxation in the crystalline arginine derivative in terms of $^{13}C$ $T_1$ relaxation "hot spots" and potential motional narrowing of chemical-shift powder patterns measured by the SUPER technique.

Note that the heteronuclear relaxation effect explored here is unrelated to the inhomogeneous line-broadening due to non-secular quadrupolar coupling acting on the heteronuclear dipolar coupling, which occurs in the absence of any motion for all $^{13}C$–$^{14}N$ spin pairs and is most pronounced at low $B_0$ field strengths [11]. In contrast, the relaxation effect of interest here requires fluctuations in the electric field-gradient tensor at the quadrupolar nucleus due to dynamic processes.

## 2. Theoretical background and simulations

To analyze heteronuclear evolution in the presence of $T_{1Q}$ relaxation, we first consider the general situation, and then simulate the specific cases of an *S-spin* coupled to an $L = 1/2$, $L = 1$, or $L = 3/2$ spin.

### 2.1. Relaxation of L-spin pseudo-populations

Using product operators for the $S$-spin and matrix representations for the $L$-spin terms, the general reduced density matrix can be written as

$$\rho(t) = S_x \mathrm{diag}(p_{x,L}, p_{x,(L-1)}, \ldots, p_{x,-(L-1)}, p_{x,-L}) + S_y \mathrm{diag}(p_{y,L}, p_{y,(L-1)}, \ldots, p_{y,-(L-1)}, p_{y,-L}) \quad (1)$$

with time-dependent pseudo-populations in the diagonal $L$-spin matrices consisting of $(2L + 1)$ columns and rows. Normally, the diagonal elements of the density matrix correspond to populations of the corresponding energy levels. However, in the present case, some of the diagonal elements are negative; therefore, we refer to them as pseudo-populations.

The exchange between the (pseudo-)populations due to longitudinal relaxation is controlled by a relaxation exchange matrix $\underline{W}$ (also denoted as $\underline{R}$ or $\underline{K}$ in the literature) [12,13].

$$dp_{x,m}/dt = \sum_{m'=-L}^{L} W_{m,m'} p_{x,m'} \quad (2)$$

The $\underline{W}$ matrices for the first three L values are [12,13]

$$\underline{W} = \begin{pmatrix} -r & r \\ r & -r \end{pmatrix} \quad (L = 1/2) \quad (3a)$$

$$\underline{W} = \begin{pmatrix} -r_1 - r_2 & r_1 & r_2 \\ r_1 & -2r_1 & r_1 \\ r_2 & r_1 & -r_1 - r_2 \end{pmatrix} \quad (L = 1) \quad (3b)$$

$$\underline{W} = \begin{pmatrix} -r_1 - r_2 & r_1 & r_2 & 0 \\ r_1 & -2r_1 - r_2 & r_1 & r_2 \\ r_2 & r_1 & -2r_1 - r_2 & r_1 \\ 0 & r_2 & r_1 & -r_1 - r_2 \end{pmatrix} \quad (L = 3/2) \quad (3c)$$

In the $\underline{W}$-matrix for $L = 3/2$, it has been taken into account that the triple-quantum (and higher) matrix elements of electric quadrupolar and magnetic dipolar relaxation vanish [14], $r_3 = 0$. The matrix elements relate to the single- and double-quantum relaxation time constants $T_{1Q}^{SQ}$ and $T_{1Q}^{DQ}$ of spin $L$ and the spectral densities of the dynamics as follows:

$$r = 1/(2T_{1L}) = \frac{3}{10}\gamma_L^2\gamma_S^2\hbar^2 r_{LS}^{-6}\left[\frac{1}{3}J(\omega_L - \omega_S) + J(\omega_S) + J(\omega_L + \omega_S)\right] \quad (4a)$$

$$r_1 = 1/(3T_{1Q}^{SQ}) = \frac{1}{8}\left(\frac{eqQ}{\hbar}\right)^2 J^{(1)}(\omega_0) \quad (4b)$$

$$r_2 = 1/(3T_{1Q}^{DQ}) = \frac{1}{4}\left(\frac{eqQ}{\hbar}\right)^2 J^{(2)}(2\omega_0) \quad (4c)$$

It has been shown that $r_1$ and $r_2$ usually do not differ greatly [15,16]. For instance, isotropic motion gives $r_1 = 2\,r_2$ in the slow-motion and $r_1 = 0.5\,r_2$ in the fast-motion regime [16]. In most of our simulations, we assume $r_1 = r_2$, but we will also explore the effects of the two rates not being equal. We have also neglected the orientation-dependence of the relaxation rates and times. For $T_{1Q} > t_r$, this effect is minor since much of the variation is averaged out by MAS.

Further, $r_1$ and $r_2$ or $T_{1Q}^{SQ}$ and $T_{1Q}^{DQ}$ should be related to the easily observable longitudinal relaxation times $T_{1L}$ of z-magnetization and $T_{1Q}$ of the spin-alignment state for $L = 1$ [16]:

$$1/T_{1L} = r_1 + 2r_2 \quad (5a)$$

$$1/T_{1Q} = 3r_1 \quad (5b)$$

When we assume $r_1 = r_2$, all these equations simplify to $T_{1L} = T_{1Q} = T_{1Q}^{SQ} = T_{1Q}^{DQ}$. On this basis, we can refer to the quadrupolar $T_{1L}$ as $T_{1Q}$ (which highlights the quadrupolar nature of the relaxation) without conflicting with the traditional definition.

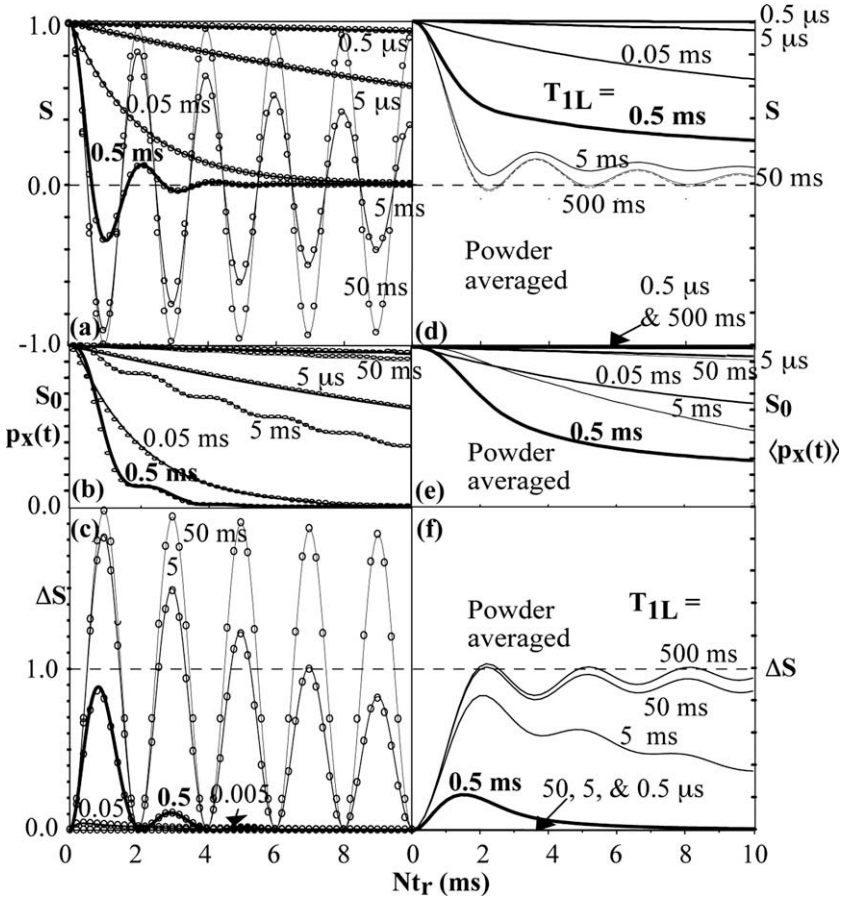


**Fig. 2.** $S\{L\}$ REDOR S, $S_0$and $\Delta S$ simulations for spin $L = 1/2$ with $T_{1L}$ relaxation. Single-frequency analytical simulations are shown in (a–c) with solid lines, numerical simulations are represented by open circles. $\omega_{SL} = 2\pi$ 1 kHz was used in both simulations. Numerical powder-averaged REDOR simulations are shown in (d–f) with $\delta_{SL} = 2\pi$ 1.5 kHz. $T_{1L}$ values are indicated at each curve.

### 2.2. Heteronuclear evolution in the presence of $T_{1Q}$ relaxation

We insert the general $\rho(t)$ of Eq. (1) into the von Neumann equation with relaxation

$$d\rho/dt = -i/\hbar[H_{SL}, \rho] + \underline{R}\rho \tag{6}$$

with the heteronuclear Hamiltonian

$$H_{SL} = \hbar\omega_{SL}S_zL_z \tag{7}$$

Under MAS and recoupling, $\omega_{SL}$ is the effective (average) frequency obtained after full rotation periods $Nt_r$. The action of the Redfield supermatrix $\underline{R}$ on the $L$-spin matrices is given by the effect of the regular matrix W on the $L$-spin population vectors, Eq. (2). As shown in Appendix A, inserting $\rho(t)$ of Eq. (1) into Eq. (6) gives coupled differential equations for the coefficients:

$$dp_{y,m}/dt = \omega_{SL}mp_{x,m} + \sum_{m'} W_{mm'}p_{y,m'} \tag{8a}$$

$$dp_{x,m}/dt = -\omega_{SL}mp_{y,m} + \sum_{m'} W_{mm'}p_{x,m'} \tag{8b}$$

The initial condition for $\rho(0) = S_x$, magnetization is $p_{x,m}(0) = 1$ and $p_{y,m}(0) = 0$. The observable magnetization is obtained from the solution according to

$$\langle S_x\rangle = tr(S_x 1_L\rho) \sim \sum_m p_{x,m}(t) \tag{9}$$

For $L = 1/2$, two of the four equations are redundant and with $p_{x,-1/2} = p_{x,+1/2} = p_x$ and $p_{y,-1/2} = -p_y$, $_{+1/2} = -p_y$ we obtain (see Appendix B)

$$dp_y/dt = p_x\omega_{SL}/2 - p_y(1/T_{2S} + 1/T_{1L}) \tag{10a}$$

$$dp_x/dt = p_y(-\omega_{SL})/2 - p_x/T_{2S} \tag{10b}$$

with transverse $T_{2S}$ relaxation of the $S$-spin added in, as in the Bloch equations. The only difference from the standard Bloch equations is that the two-spin coherence $S_yL_z$ relaxes with the sum of the transverse relaxation rate of $S_y$ and the longitudinal relaxation rate of $L_z$. Similar "asymmetric relaxation" is also found in rotational resonance [17], spin exchange [18,19] and in cross polarization, with the same transition from oscillatory to exponential solutions.

Analytical solutions of Eq. (10) for the initial condition $p_x(0) = 1$, $p_y(0) = 0$ are given in Appendix B and plotted in Fig. 2a for a series of $T_{1L}$ values with $\omega_{SL} = 2\pi$ 1 kHz. For $T_{1L} > T_{2S} > 1/\omega_{SL}$ the solution is the expected slightly damped $\cos(\omega_{SL}/2t)$ oscillation, but for $T_{1L} < 1/\omega_{SL}$ it changes to a biexponential monotonous decay. For very short $T_{1L}$, a slow exponential decay is observed,

$$S(t) = \exp(-\omega_{SL}^2T_{1L}t/4) \tag{11}$$

as shown in Appendix C. With the decay constant in Eqs. (11) and (C1b) inversely proportional to $T_{1L}$, the decay becomes negligible for extremely short $T_{1L}$, i.e. self-decoupling is reproduced.

For $L > 1/2$, the analytical solutions are more complicated [8], and we have chosen instead to evaluate Eq. (8) numerically as outlined at the end of Appendix A. Sample results are plotted in Fig. 3a for $L = 1$, and Fig. S1a for $L = 3/2$.

The consistency of the numerical simulations with the analytical simulations for $L = 1/2$ confirms their accuracy. These simulations used a single-frequency, which is relevant for dipolar

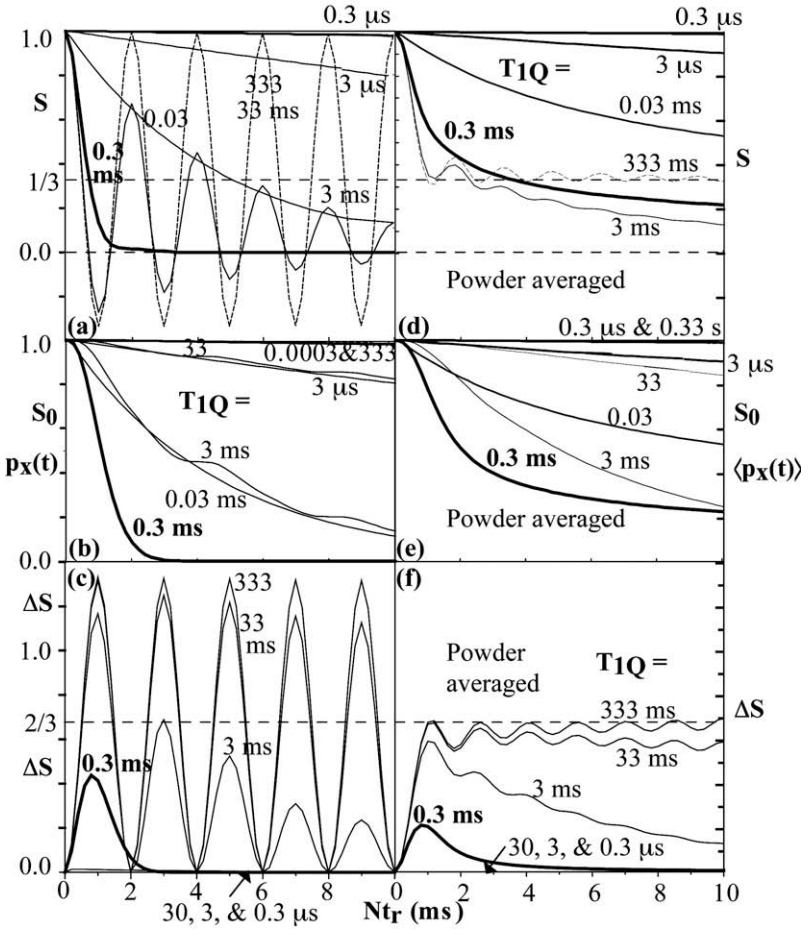


**Fig. 3.** $S\{L\}$ REDOR simulations for spin $L = 1$ with $T_{1Q}$ relaxation. Single-frequency REDOR (a) $S$, (b) $S_0$, and (c) $\Delta S$ simulations with $\omega_{SL} = 2\pi$ 1.5 kHz. Powder-averaged REDOR (d) $S$, (e) $S_0$, and (f) $\Delta S$ simulations with $\delta_{SL} = 2\pi$ 1.5 kHz.

coupling in single crystals and, more importantly, for a strong $J$-coupling to the quadrupolar nucleus (see discussion below). For long $T_{1Q}$, we should recover the normal evolution

$$\rho(t) = S_x \sum_{m=0\text{ or }1/2}^{L} \underline{1}_m \cos(m\omega_{SL}t) + S_y L_z \sum_{m=0\text{ or }1/2}^{L} \frac{1}{m}\underline{1}_m \sin(m\omega_{SL}t) \qquad (12)$$

where $\underline{1}_m$ is a diagonal matrix with vanishing elements except for ones on the diagonal $m$-position and $-m$-position. For $m = 0$, the second term in Eq. (12) vanishes. Eq. (12) gives the expected signals

$$S(t) = 1/3 + 2/3\cos(\omega_{SL}t) \quad (L = 1, T_{1Q} \gg 2\pi/\omega_{SL}) \qquad (13a)$$

$$S(t) = 1/2\cos(\omega_{SL}t/2) + 1/2\cos(3\omega_{SL}t/2) \quad (L = 3/2, T_{1Q} \gg 2\pi/\omega_{SL}) \qquad (13b)$$

seen in Figs. 3a and S1a for long $T_{1Q}$. Simulated curves with powder averaging are shown in Figs. 2d, 3d, and S1d, for $\delta_{SL} = 2\pi$ 1.5 kHz. For $L = 1/2$ and 1 at long $T_{1Q}$, they reproduce the shape of the familiar REDOR curve. For $L = 1$, the long-time plateau is at an intensity of 1/3 (see Eq. (13a)) due to the $m = 0$ component with frequency 0. At intermediate $T_{1Q}$ values, the plateau slopes to 1/9 because of relaxation of the $L_z^2$ term of the $m = 0$ component in $S_x(1 - L_z^2)$ [12,13].

### 2.3. Refocusing of recoupling

In recoupling of heteronuclear interactions of an $S$-spin to an $L$-spin with a spectrum too broad for a train of inversion pulses, the recoupling pulses need to be applied to the $S$-spin; the reference signal $S_0$ is obtained by refocusing the recoupling effect, see Fig. 1. In the center of the $S_0$ pulse sequence, at $t = Nt_r/2$, a 180° pulse is "missing", inverting the effective frequency. Thus, in the second half of the sequence, Eqs. (8a) and (8b) apply with $\omega_{SL}$ replaced by $-\omega_{SL}$. The intensity of the observable signal $S_0(Nt_r, T_{1Q})$ for $L = 1/2$ and different $T_{1L}$ values, calculated in Appendix B, is shown in Fig. 2b and coincides with the numerical results. Numerical simulations for $L = 1$ and $L = 3/2$ are plotted in Figs. 3b and S1b, respectively. Corresponding powder averaged $S_0$ curves are shown in Figs. 2e, 3e, and S1e, with $\delta_{SL} = 2\pi$ 1.5 kHz.

Interestingly, noticeable oscillations with a frequency of $1/2\ m\omega_{SL}$ are observed in the $S_0$ curves at long to intermediate $T_{1Q}$ values, in particular in Figs. 2b and 3b. It appears that the magnetization at $Nt_r$ to some extent reflects the magnetization at $Nt_r/2$, the time of the inversion of the effective frequency.

### 2.4. $T_{1Q}$ effect on $\Delta S$

$\Delta S$ is obtained by subtracting $S$ from $S_0$, representing the dephasing due to heteronuclear recoupling. The simulated $\Delta S$ curves for various $T_{1Q}$ values are presented in Figs. 2c, 3c, and S1c for a single-frequency $\omega_{SL}$ and in Figs. 2f, 3f, and S1f for powder averaging with $\delta = 2\pi$ 1.5 kHz. These $\Delta S$ curves for $L = 1/2$, 1, and 3/2 show similar patterns: In powder averaged simulations, for long $T_{1Q} > 100/\delta$, the intensity of $\Delta S$ quickly rises to the maximum and then slightly oscillates around the plateau value, which is the ideal case for experiments like SPIDER, REDOR, and REAPDOR. For $T_{1Q} \approx 100/\delta$, the maximum is reduced by about 20% compared to the ideal value and the intensity decays fast after reaching the

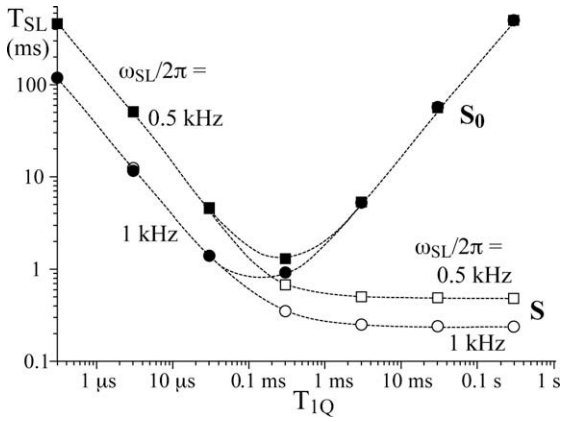


**Fig. 4.** Decay time constants $T_{SL}$ of REDOR $S$ and $S_0$ for spin $L = 1$ as a function of $T_{1Q}$, with two different coupling strengths, $\omega_{SL} = 2\pi$ 0.5 kHz and $\omega_{SL} = 2\pi$ 1 kHz.

maximum. For $T_{1Q} < 10/\delta$, the maximum intensity is reduced by more than 70%. For $T_{1Q} \ll 1/\delta$, in the self-decoupling limit, no $\Delta S$ signal can be obtained. In single-frequency simulations, see Figs. 2c, 3c, and S1c, the amplitude of the oscillations is damped quickly as $T_{1Q}$ decreases, until no intensity is observed when $T_{1Q}$ is extremely short.

### 2.5. $T_{1Q}$ dependence of REDOR decay time constants in $S_0$ and $S$

Decay time constants $T_{SL}$ were extracted from the simulated single-frequency REDOR $S$ and $S_0$ curves for spin $L = 1$ shown in Fig. 3a and b, and plotted as a function of $T_{1Q}$ in Fig. 4, for coupling strengths of $\omega_{SL} = 2\pi$ 1 kHz and $2\pi$ 0.5 kHz. For our purpose, $T_{SL}$ was defined simply as the time of the initial decrease of the intensity to $e^{-1} = 0.37$. For small $T_{1Q} \ll 1/\omega_{SL}$, $T_{SL}$ increases as $T_{1Q}$ decreases, approaching more and more complete self-decoupling. In this range, the $S$ and $S_0$ curves coincide: The only difference between $S$ and $S_0$ in REDOR is the inversion pulse in the middle of the recoupling period in $S$ but not in $S_0$, which inverts the $S$–$L$ coherence. If that coherence decays completely before the inversion or saturation pulse, then there will be no difference between $S$ and $S_0$. $T_{SL}$ values are seen to be inversely proportional to $T_{1Q}$ and to the square of the coupling strength. These power laws can be derived by analytical calculations for $L = 1/2$, see Appendix C.

At $T_{1Q} = 1/\omega_{SL}$, $S_0$ has a minimum for both coupling strengths, and the decrease in $T_{SL}$ for $S$ starts to level off. For $T_{1Q} > 1/\omega_{SL}$, the $T_{SL}$ values for the $S$ signal approach plateaus independent of $T_{1Q}$. This is the standard regime with negligible effects of $T_{1Q}$ on the REDOR decay. The heights of the plateaus are inversely proportional to the coupling strengths, as expected since a larger coupling strength will produce a faster initial decay (as part of the cosine oscillation) and thus a shorter decay constant $T_{SL}$.

Further, the plot shows that $T_{SL}$ for $S_0$ increases as $T_{1Q} > 1/\omega_{SL}$ increases and values for different coupling strengths merge on a line $T_{SL} = 2T_{1Q}$. Again, this power law has been derived for spin-1/2 in Appendix C. Qualitatively, one can say that for longer $T_{1Q}$, a larger part of the $S$–$L$ coherence can be refocused, independent of coupling strength, before it has relaxed, so $S_0$ decays more slowly as $T_{1Q}$ increases.

### 2.6. Different double- and single-quantum relaxation times

So far, we have assumed that the double-quantum and single-quantum relaxation rates are equal. In order to explore their independent effects, Fig. 5a displays a contour plot of $\log T^0_{SL}$ as a function of $\log(T^{SQ}_{1Q})$ and $\log(T^{DQ}_{1Q})$ for the $S$ decay in REDOR for $L = 1$. Fig. 5b shows the corresponding plot of $\log T_{SL}$ of the $S_0$ intensity. The plots show that (i) ideal REDOR with long $T^0_{SL}$ is recovered only if both $T^{SQ}_{1Q}$ and $T^{DQ}_{1Q}$ are long (upper right corner); (ii) self-decoupling (both $T^0_{SL}$ and $T_{SL}$ are long) will occur if at least one relaxation time is short, and $T^{DQ}_{1Q}$ is more effective at producing self-decoupling; (iii) if both $T^0_{SL}$ and $T_{SL}$ are short, one of them must be between $1/(2\ \omega_{SL})$ and $3/\omega_{SL}$ and the other longer than $1/(2\ \omega_{SL})$.

As mentioned above, $T^{SQ}_{1Q}$ and $T^{DQ}_{1Q}$ are typically not very different. The dashed lines in Fig. 5 delineate the expected range of $T^{SQ}_{1Q} \approx T^{DQ}_{1Q}$ values. The curves of $\log T^0_{SL}$ and $\log T_{SL}$ as a function of $\log(T_{1Q})$ shown in Fig. 4 are found along the diagonals $(T^{SQ}_{1Q} = T^{DQ}_{1Q})$ of the contour plots of Fig. 5, with a plateau in $T^0_{SL}$ at large $T^{SQ}_{1Q} = T^{DQ}_{1Q}$ values and a minimum in $T_{SL}$ near the center of the plot. The behavior within the dashed lines is qualitatively similar as along the corresponding diagonal.

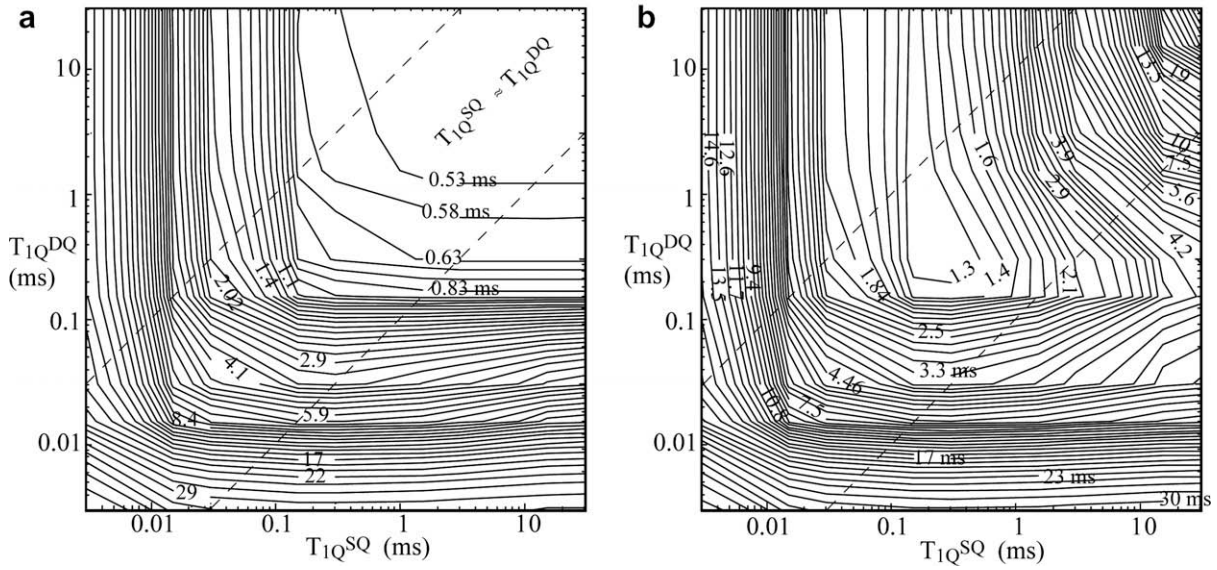


**Fig. 5.** Contour plots of (a) $T_{SL}$ for REDOR $S$ decay and (b) $T^0_{SL}$ for REDOR $S_0$ decay as a function of $T^{SQ}_{1Q}$ and $T^{DQ}_{1Q}$ on a logarithmic scale, for $L = 1$. The coupling strength is $\omega_{SL} = 2\pi$ 0.5 kHz.

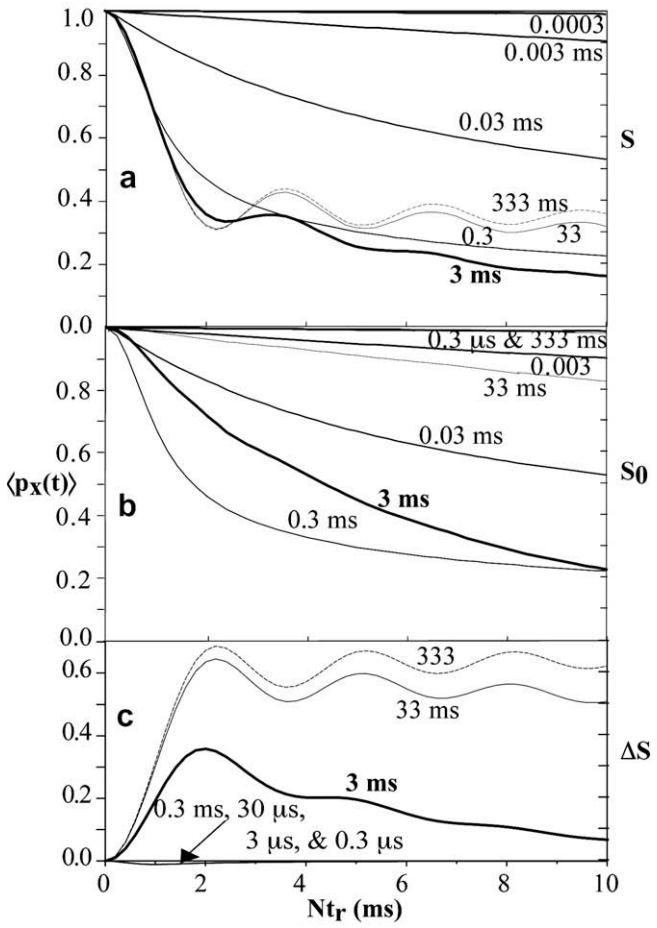


**Fig. 6.** $S\{L\}$ SPIDER simulations for $L = 1$ with $T_{1Q}$ relaxation and powder averaging, for a coupling strength $\delta_{SL} = 2\pi$ 1.5 kHz, and with 0.8-ms irradiation on the $L$-spin. (a) $S$, (b) $S_0$ and (c) $\Delta S$.

### 2.7. Heteronuclear evolution in the SPIDER experiment

In the SPIDER pulse sequence shown in Fig. 1b, the SPIDER $S$ signal is obtained after applying irradiation on the $L$-spin, which destroys the $L_z$ terms in conjunction with the strong quadrupolar coupling. The dephasing of $^{13}C$ signal by adjacent quadrupolar nuclei is accomplished during the following recoupling period. The $\pi/2$ pulse before the period of $^{14}N$ irradiation stores one component of the $^{13}C$ magnetization along z so that it relaxes more slowly, while the second $\pi/2$ pulse returns it to the transverse plane. In SPIDER $S_0$, there is no irradiation on the quadrupolar nucleus and the recoupling of $^{13}C$–$^{14}N$ is refocused by the end of the second half recoupling period. The difference $\Delta S = S_0 - S$ plotted as a function of $Nt_r$ reveals the coupling strength between $^{13}C$ and the quadrupolar nucleus $^{14}N$. In fact, this is not true when $T_{1Q}$ is short. Our powder-averaged simulations with $\delta_{SL} = 2\pi$ 1.5 kHz shown in Fig. 6 indicate that only for $T_{1Q} > 100$ ms, it shows the expected difference between $S_0$ and $S$. The effects of $T_{1Q}$ relaxation in SPIDER become significant already at longer $T_{1Q}$ times than in REDOR. Most importantly, the heteronuclear evolution in SPIDER is effectively only half as fast as in REDOR [5]. In addition, the $S_0$ signal decays faster in SPIDER than in REDOR due to $T_{1Q}$ relaxation during the 0.8-ms period for $L$-spin irradiation (which, of course, is applied only when $S$ is measured, see Fig. 1). As a result, shorter $T_{1Q}$ strongly reduces the $\Delta S = S_0 - S$ intensity, especially when $T_{1Q} \leqslant 1$ ms, where $S_0 \approx S$; this is apparently the case for the 159 and 56 ppm $^{13}C$ sites in Boc—Arg(Z)$_2$—OH, showing $\Delta S = S_0 - S \approx 0$ in Fig. 11b below.

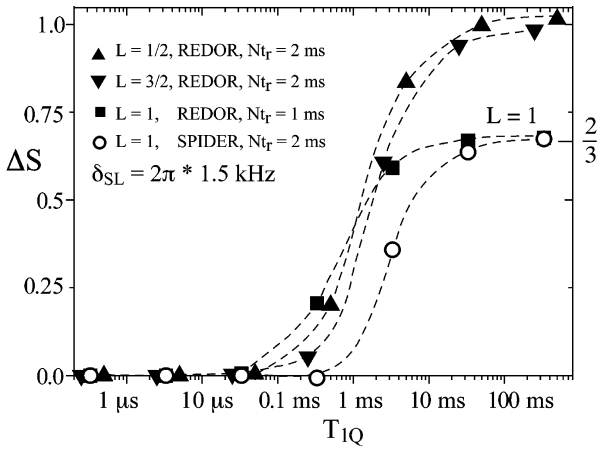


**Fig. 7.** $T_{1Q}$ dependence of $\Delta S$ intensities extracted from REDOR and SPIDER simulations with $\delta_{SL} = 2\pi$ 1.5 kHz. Filled triangles: $S\{L\}$ REDOR $\Delta S$ for spin $L = 1/2$, at recoupling time of $Nt_r = 2$ ms. Filled inverted triangles: $S\{L\}$ REDOR $\Delta S$ for spin $L = 3/2$, at $Nt_r = 2$ ms. Filled squares: $S\{L\}$ REDOR $\Delta S$ for spin $L = 1$, at $Nt_r = 1$ ms. Open circles: $S\{L\}$ SPIDER $\Delta S$ for spin $L = 1$, at $Nt_r = 2$ ms.

The effects of $T_{1Q}$ on the theoretical maximum $\Delta S$ intensity that can be obtained by REDOR experiments for $L = 1/2$, 1 and 3/2, and by SPIDER experiments for $L = 1$ are indicated in Fig. 7. For very short $T_{1Q}$ $\Delta S$ remains vanishingly small due to self-decoupling; for intermediate $T_{1Q}$, $\Delta S$ increases significantly as $T_{1Q}$ increases. For long $T_{1Q} > 100/\delta$, $\Delta S$ asymptotically approaches its maximum value, which is 1 for $L = 1/2$ and $L = 3/2$, and 2/3 for $L = 1$.

### 2.8. Design of pulse sequences for $S_{00}$

The $T_{1Q}$ relaxation effect during the $S_0$ pulse sequence, see Fig. 8a, is significant due to the continuous recoupling of the $SL$ interactions during each of the two halves of the pulse sequence. The phase

$$\Phi_{SL}(t) = \int_0^t \omega_{SL}(t')dt' \tag{14}$$

keeps growing to N $\Phi_{SL}(t_r/2)$ at $Nt_r/2$. The two-spin coherence, which is proportional to sin $\Phi_{SL}(t)$, grows accordingly. The larger the $S$–$L$ coherence, the larger will be the effect of $T_{1Q}$ relaxation of the $L$-component of that coherence. If generation of $S$–$L$ coherence could be avoided, $T_{1Q}$ relaxation would have no effect.

This undesirable signal reduction can be minimized in a pulse sequence without significant long-time recoupling. The simplest such sequence would be a $Nt_r/2$ – $\pi$-pulse – $Nt_r/2$ Hahn-spin-echo sequence. Note that even here, the $S$–$L$ coherence is generated transiently, with the maximum phase $\Phi_{SL}(t_r/2)$ in the middle of each rotation period. More importantly, the signal from this sequence will not be directly comparable with $S$ or $S_0$, since those signals are obtained after many more $\pi$-pulses. Due to the effects of imperfect $^1H$-decoupling during the pulses, pulse flip-angle errors, resonance offset, etc., the decay of $S_0$ is much faster than $T_2$ relaxation.

Therefore, we designed pulse sequences with the same number of 180° pulses as that for $S$ and $S_0$ but minimal $S$–$L$ recoupling. The most successful example is shown in Fig. 8b. It features two rotation-synchronized Hahn-echoes, at the beginning and end. Around the center, 180° pulses are applied every $t_r/3$ for four rotation periods, so that at the center, $\Phi_{SL}(Nt_r/2) = 0$. Due to the fast alternation of the sign of the effective frequency imposed by the relatively closely-spaced 180° pulses, the phase $\Phi_{SL}$ remains small throughout the whole recoupling period. Evolutions of the phase $\Phi_{SL}$ under REAPDOR or SPIDER $S$ and $S_0$ pulse sequences as well as the newly

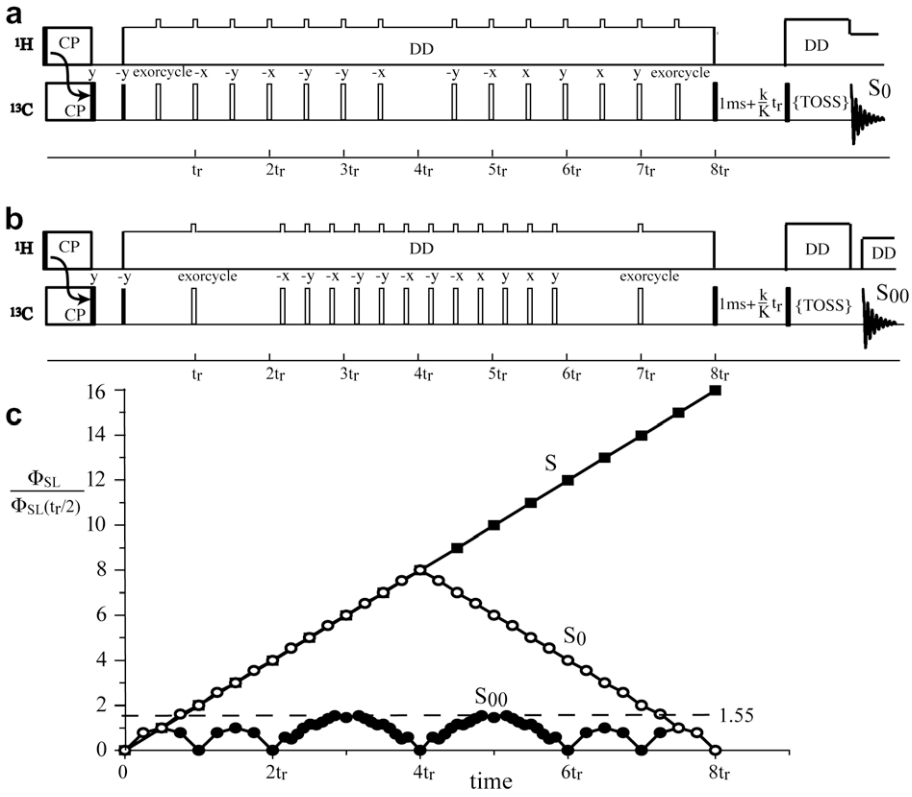


**Fig. 8.** (a) Simplified pulse sequence for measuring $S_0$ without irradiation on the quadrupolar nucleus. (b) Matching pulse sequence for measuring an improved reference signal $S_{00}$ with minimal transient *S*–*L* recoupling. (c) Simulated evolutions of the phase $\Phi_{SL}$ of the magnetization in REAPDOR or SPIDER *S* dephasing (*S*), REAPDOR or SPIDER reference experiments ($S_0$) and for the new pulse sequence shown in (b) ($S_{00}$). The unit used is the phase $\Phi_{SL}(t_r/2)$ generated within half a rotation period ($t_r/2$) under free evolution.

designed $S_{00}$ sequence, calculated using the SIMPSON program [20], are shown in Fig. 8c. While for REDOR $S_0$, $\Phi_{SL}$ reaches a large value of $8\Phi_{SL}(t_r/2)$ at $Nt_r/2$, $\Phi_{SL}$ is seen to be always comparable or smaller than 1.55 $\Phi_{SL}(t_r/2)$ during the $S_{00}$ pulse sequence; for reference, free evolution gives a maximum of 1.0 $\Phi_{SL}(t_r/2)$. Independent EXORCYCLEs [21] of the first and last 180° pulses (in the Hahn-echo part of the sequence) were employed. The same phase sequence and phase cycle were applied in the $S_0$ pulse sequence, which actually appeared to increase the $S_0$ intensity compared to an incomplete xy phase sequence on all fourteen 180° pulses. We also designed and tested many other pulse sequences with some smaller pulse spacings than shown in Fig. 8b, but they did not work as well as the one presented here, in particular being more narrowband.

The signal obtained with minimum recoupling is termed $S_{00}$. The $S_{00}$ and $S_0$ spectra match well near resonance (within ±1 kHz). In our experiments, the match of the $S_{00}$ and $S_0$ spectra was found to remain good (within ±4%) down to −12 kHz downfield from resonance, while it degraded markedly for offsets >+1 kHz upfield from resonance. The reason for this asymmetry, which was similar for different xy-8 sequences (e.g. x y x y; x –y x –y; and –x –y –x –y), remains unclear. The $S_{00}$ sequence produced reduced C—H dephasing, resulting in ~10% higher signals of CH groups. This was compensated empirically by 6 μs of dipolar dephasing before detection, for all samples measured.

Table 1 provides an overview of the intensities of *S*, $S_0$, and $S_{00}$ for various $T_{1Q}$ regimes. The entries are based on the curves in Figs. 3, 6 and 7 (for *S*, $S_0$, and $\Delta S$) and on the experimental observations for $S_{00}$. In the regime with negligible relaxation, $T_{1Q} > 100/\delta$, we have $S_{00} = S_0$, otherwise, $S_{00} > S_0$. Finally, for $T_{1Q} \ll 1/\delta$, self-decoupling is reached, where there is hardly any heteronuclear evolution before the spin state of the quadrupolar nucleus relaxes and therefore no $^{13}C$–$^{14}N$ correlation can be detected. $\Delta S_0$ represents the improvement of signal intensity made by using the new pulse sequence. However, directly obtaining the full $\Delta S_{tot}$ in one spectrum by combining the new $S_{00}$ pulse sequence with SPIDER dephasing in *S* is experimentally very challenging for demanding samples like natural organic matter, because the artifacts from a few percent of

**Table 1**
Table of normalized SPIDER S, $S_0$, $S_{00}$, $\Delta S = S_0 - S$, $\Delta S_0 = S_{00} - S_0$, and $\Delta S_{tot} = S_{00} - S$ intensities for long ($T_{1Q} > 100/\delta$), intermediate ($10/\delta < T_{1Q} < 100/\delta$), short ($1/\delta < T_{1Q} < 10/\delta$), very short ($T_{1Q} \sim 1/\delta$), and extremely short ($T_{1Q} \ll 1/\delta$) quadrupolar relaxation times, for $L = 1$ and $Nt_r = 20/\delta$. Note that the definition of the *S*–*L* dipolar coupling constant $\delta$ includes the factor $2\pi$.

| Signal | $S_{00}$ | $S_0$ | $S$ | $\Delta S$ | $\Delta S_0$ | $\Delta S_{tot}$ |
|---|---|---|---|---|---|---|
| $T_{1Q}$ | | | | | | |
| Long ($T_{1Q} > 100/\delta$) | 1 | 1 | 0.33 | 0.67 | 0 | 0.67 |
| Intermediate ($10/\delta < T_{1Q} < 100/\delta$) | ~0.9 | ~0.8 | ~0.4 | ~0.4 | ~0.1 | ~0.5 |
| Short ($1/\delta < T_{1Q} < 10/\delta$) | ~0.8 | ~0.5 | ~0.5 | ~0 | ~0.3 | ~0.3 |
| Very short ($T_{1Q} \sim 1/\delta$) | ~0.8 | ~0.7 | ~0.7 | 0 | ~0.1 | ~0.1 |
| Extremely short ($T_{1Q} \ll 1/\delta$) | ~1 | ~1 | ~1 | 0 | 0 | 0 |

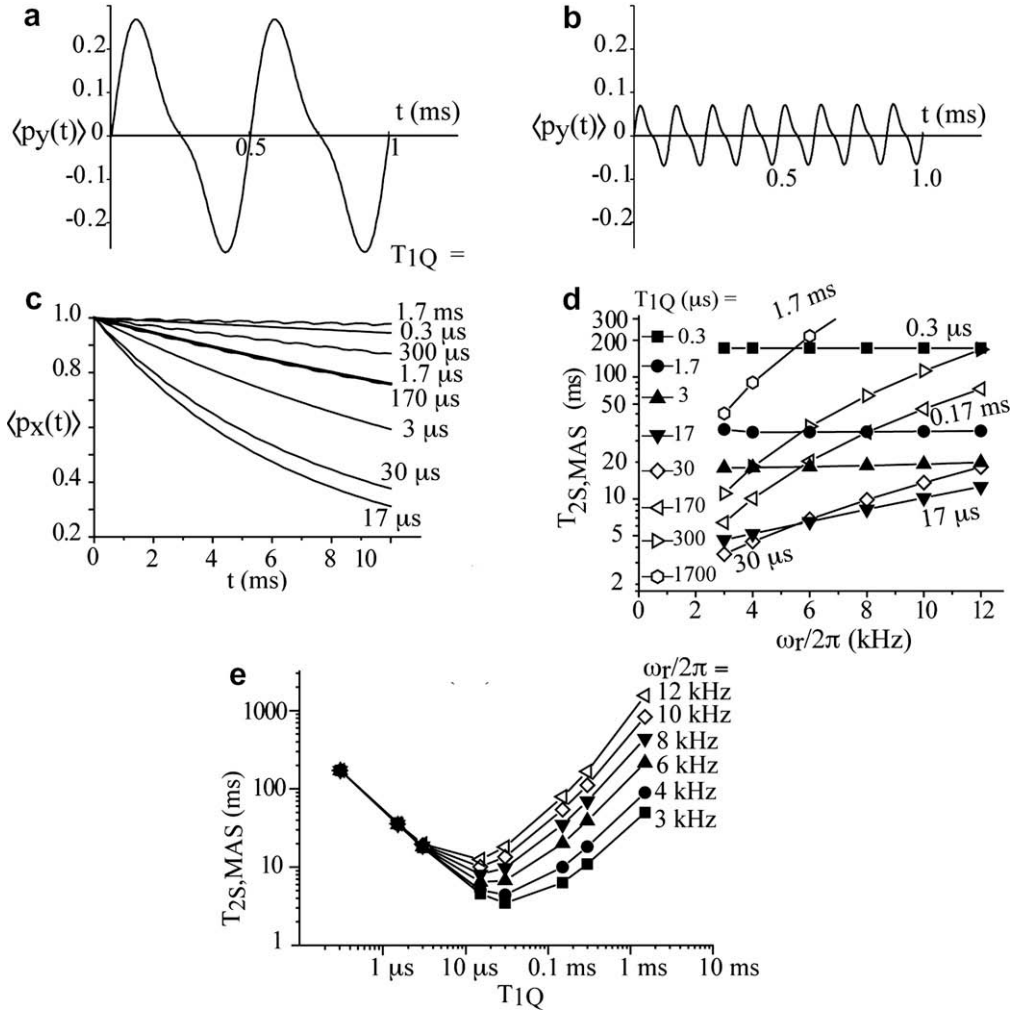


**Fig. 9.** Effects of $T_{1Q}$ relaxation during free MAS, calculated for $L = 1$. (a and b) Amplitude of the two-spin coherence of heteronuclear evolution simulated with long $T_{1Q} = 333$ ms under magic angle spinning (MAS) of (a) 2 kHz and (b) 8 kHz. (c) Simulated $T_{2S,MAS}$ decay at 8 kHz without recoupling, for various $T_{1Q}$ values. (d) Spinning-frequency dependence of $T_{2S,MAS}$ for various values of $T_{1Q}$ in ms as shown in the figure. $\omega_{SL} = 2\pi$ 1.5 kHz was used in the simulations. (e) $T_{1Q}$ dependence of $T_{2S,MAS}$ at various spinning frequencies.

mismatch between $S_{00}$ and $S_0$ will be comparable to the desired signal $\Delta S_{tot}$.

### 2.9. $T_{1Q}$-enhanced, $\omega_r$-dependent $T_{2S,MAS}$ relaxation

Even during free MAS without recoupling pulses, the effect of $T_{1Q}$ relaxation on the heterogeneous evolution may be detectable. During the course of each rotation period $t_r$, $S_yL_z$ coherence is generated at the expense of $S_x$ and relaxes towards zero. By the end of the rotation period, the two-spin coherence is reconverted into magnetization, but less so if the two-spin coherence has been depleted by relaxation. This speeds up the effective $T_2$ relaxation of the observed $S$-spin. The evolution at the beginning of each rotation period is the same (in the quasistatic regime) but is terminated the earlier, the shorter the rotation period, since the initial state must be recovered at the end of the rotation period. Therefore, the longer the rotation period, the greater the two-spin coherence will become, see Fig. 9a and b. As a result, the effective $T_2$ relaxation time of the $S$-spin ($T_{2S,MAS}$) will decrease markedly with increasing $t_r$ and decreasing spinning-frequency.

The dependence of $T_{2S,MAS}$ on the spinning-frequency $\omega_r$, relaxation time $T_{1Q}$, and coupling constant $\delta_{SL}$ can be predicted using numerical simulation. The time-dependent frequency during free MAS can be written as:

$$\omega_{SL}(t) = C_1\cos(\gamma + \omega_r t) + C_2\cos(2\gamma + 2\omega_r t) + S_1\sin(\gamma + \omega_r t) + S_2\sin(2\gamma + 2\omega_r t) \quad (15)$$

For a spin-pair dipolar coupling, $S_1 = S_2 = 0$, [22] and

$$C_1 = -\delta_{SL}\sqrt{2}/2\sin(2\beta) \quad (16a)$$

$$C_2 = \delta_{SL}/2\sin^2\beta \quad (16b)$$

We use $\omega_{SL}(t)$ instead of the constant $\omega_{SL}$ in Eq. (8) and evaluate the evolution numerically as outlined in Appendix A, Eq. (A4). Powder averaging is performed by adding curves for $\beta = 0°, \ldots, 90°$ with $\sin\beta$ weighting. The effect of $\gamma$ on the simulations is minimal, since all values of $\gamma + \omega_r t$ are scanned in the course of each rotation period.

### 2.10. Parameter dependencies of $T_{2S,MAS}$

At a fixed spinning-frequency (8 kHz), the $T_{2S,MAS}$—relaxation time decreases with decreasing $T_{1Q}$ and increases when $T_{1Q} < 20$ µs (see simulations for $L = 1$ in Fig. 9c), due to the loss of heteronuclear coherence. Fig. 9d illustrates that $T_{2S,MAS}$ increases with spinning-frequency for constant $T_{1Q}$. This effect is more pronounced when $T_{1Q}$ is relatively long. However, when $T_{1Q}$ is smaller than 3 µs, $T_{2S,MAS}$ is almost independent of spinning-frequency,

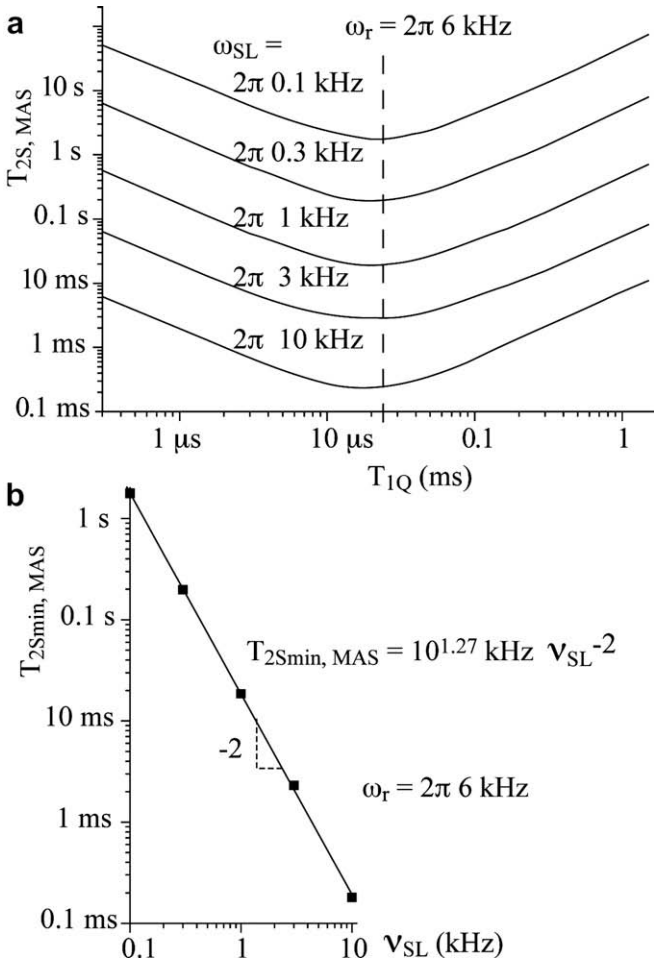


**Fig. 10.** (a) Simulated $T_{1Q}$ dependence of $T_{2S,MAS}$ with various coupling strengths. (b) Plot of minimum $T_{2S,MAS}$ vs. coupling strength $\nu_{SL}$. The relationship between $T_{2Smin,MAS}$ and $\nu_{SL} = \omega_{SL}/2\pi$ kHz obtained from the fit is: $T_{2Smin,\ MAS} = 10^{1.27}$ kHz * $(1/\nu_{SL})^2$. The simulations were carried out for a spinning-frequency of $\omega_r = 2\pi$ 6 kHz.

increasing by only 0.1% from 3 to 12 kHz: The two-spin coherence $S_yL_z$ relaxes so fast that it does not accumulate significantly during one rotation period, even at low spinning speed, and therefore, it shows little dependence on the spinning speed. The effect of $T_{1Q}$ on $T_{2S,MAS}$ for different spinning speeds is shown in Fig. 9e. Generally, in the short-$T_{1Q}$ regime, $T_{2S,MAS}$ decreases as $T_{1Q}$ increases, due to the increased coupling generating large two-spin coherence term $S_yL_z$ combined with fast relaxation of $L_z$; in the long-$T_{1Q}$ regime of spin $L$, $T_{2S,MAS}$ increases with $T_{1Q}$, due to the slow-down of the decay of the two-spin coherence term $S_yL_Z$. At a higher spinning speed, the $T_{2S,MAS}$ minimum value is larger and appears at a smaller $T_{1Q}$ than that for slower spinning.

The $\omega_{SL}$ dependence of $T_{2S,MAS}$ relaxation was also explored in simulations for a fixed spinning speed of $2\pi$ 6 kHz, see Fig. 10. Fig. 10a shows the $T_{1Q}$-dependence of $T_{2S,MAS}$ for coupling strengths between $2\pi$ 0.1 kHz and $2\pi$ 10 kHz. The curves of log $T_{2S,MAS}$ vs. log $T_{1Q}$ have approximately the same shape, with minima fixed at $T_{1Q} = 1/(2\pi\ 6\ \text{kHz}) = 27\ \mu\text{s}$ for $\omega_{SL} < \omega_r$, see Fig. 10a. This is due to the evolution being mainly modulated by $\omega_r$ when $\omega_{SL} \ll \omega_r$. As a result, the largest effects of $T_{1Q}$ relaxation are observed for smaller $T_{1Q}$ values in free MAS (with $\omega_r$ modulation) than in recoupling experiments (with $\omega_{SL}$ modulation), since in practice usually $\omega_{SL} < \omega_r$. For $\omega_{SL} = 2\pi$ 10 kHz > $\omega_r$, a slight horizontal shift of the minimum is observed: When $\omega_{SL} \gg \omega_r$, the evolution of the two-spin coherence is modulated by $\omega_{SL}$ and the $T_{2S,MAS}$ minimum position will be $\omega_{SL}$-dependent. The depth of the minimum depends strongly on the coupling strength $\nu_{SL} = \omega_{SL}/2\pi$. Linear fitting shows an inverse-square dependence of $T_{2S,MAS}$ on $\nu_{SL}$, $T_{2min} = 10^{1.27}$ kHz $(1/\nu_{SL})^2$, see Fig. 10b.

## 3. Experimental results and discussion

### 3.1. "Missing signals" in $^{13}C\{^{14}N\}$ SPIDER NMR

CP/TOSS and SPIDER spectra of Boc—Arg—OH and Boc—Arg(Z)$_2$—OH are shown in Fig. 11a and b, respectively. In the $\Delta S$ SPIDER spectrum of Boc—Arg—OH, all the expected signals of C bonded to N are observed. By contrast, the chemically similar Boc—Arg(Z)$_2$—OH does not produce the expected $\Delta S$ peaks for the C=O and C—H carbons bonded to the "backbone" N. A twofold signal reduction was also observed in the SPIDER $\Delta S$ spectrum of chitin, an *N*-acetylated polysaccharide that forms the exoskeleton of arthropods, see Fig. 5 of Ref. [5]. In the following, we prove that these signal losses are due to relaxation of the $^{14}$N spin state during the $S_0$ pulse sequence, and demonstrate the predicted unusual $T_{2S,MAS}$ behavior for these same carbon sites.

### 3.2. Measurement of $\Delta S_0$ from $S_{00}$ and $S_0$ spectra

$S_{00}$ spectra of Boc—Arg—OH and Boc—Arg(Z)$_2$—OH with minimal recoupling are displayed in Fig. 12, measured with the new pulse sequence shown in Fig. 8b. They are compared with $S_0$ spectra obtained using the matching pulse sequence of Fig. 8a. The difference $\Delta S_0 = S_{00} - S_0$ reveals signals loss due to $T_{1Q}$ relaxation during the refocused recoupling. The intensity of $\Delta S_0$ matches the $S_0$ intensity loss in the SPIDER experiments, in particular for the bands of Boc—Arg(Z)$_2$—OH at 159 and 56 ppm, which are due to the carbons bonded to the "backbone" nitrogen. This provides an experimental confirmation of our hypothesis that the reduced $S_0$ intensity in the SPIDER spectra is due to transient recoupling to a $^{14}$N with short $T_{1Q}$.

The observed $\Delta S_0/S_{00}$ and $\Delta S/S_0$ values enable us to estimate $T_{1Q}$, based on the curves of Fig. 6. The small $\Delta S$ signal at 159 and 56 ppm indicates that $T_{1Q} \leqslant 0.3$ ms, according to Fig. 6c. The experimentally observed significant decay of $S_0$ shows that the self-decoupling regime has not been reached, $T_{1Q} \geqslant 0.3$ ms, according to Fig. 6b.

The $S_{00}$, $S_0$, and $\Delta S_0$ spectra of chitin, an *N*-acetylated polysaccharide, and of the oligopeptide, $(POG)_{10}$, are shown in Fig. 13. For chitin, the considerable $\Delta S_0$ intensity for the signals of the two carbons bonded to N proves that the weak SPIDER $\Delta S$ signal found in Ref. [5] is caused by the reduced intensity of $S_0$. The observed dephasing, $\Delta S/S_0 \sim 0.25$ and $\Delta S_0/S_{00} \sim 0.25$, indicates that 0.3 ms < $T_{1Q}$ < 1 ms. For $(POG)_{10}$, intense signals of all carbons connected to N show up in the $\Delta S_0$ spectrum, indicative of short $T_{1Q}$ between 0.2 and 1 ms for proline and hydroxyproline N in the peptide.

For carbon sites close to quadrupolar spins with sufficiently long $T_{1Q}$ > 10 ms, recoupling techniques such as SPIDER, REAPDOR or TRAPDOR give the expected results; $^{13}$C sites close to $^{14}$N nuclei in Boc—Arg—OH are examples. Nevertheless, even for these carbons, the non-zero $\Delta S_0$ intensity also indicates a slight intensity reduction of $S_0$. Adaptations of the new $S_{00}$ pulse sequence for SPIDER, REAPDOR, or RIDER experiments would facilitate applications of these methods to systems with short $T_{1Q}$ relaxation times. The challenge consists in matching $S_{00}$ and $S$ pulse sequences well enough to make the artifact difference signals much smaller than those of the nitrogen-bonded carbons.

### 3.3. $T_{1Q}$-enhanced $T_{2S,MAS}$ relaxation

The effect of the fast $T_{1Q}$ relaxation of the "backbone" N of Boc—Arg(Z)$_2$—OH on the $T_{2S,MAS}$ relaxation time of the neighboring

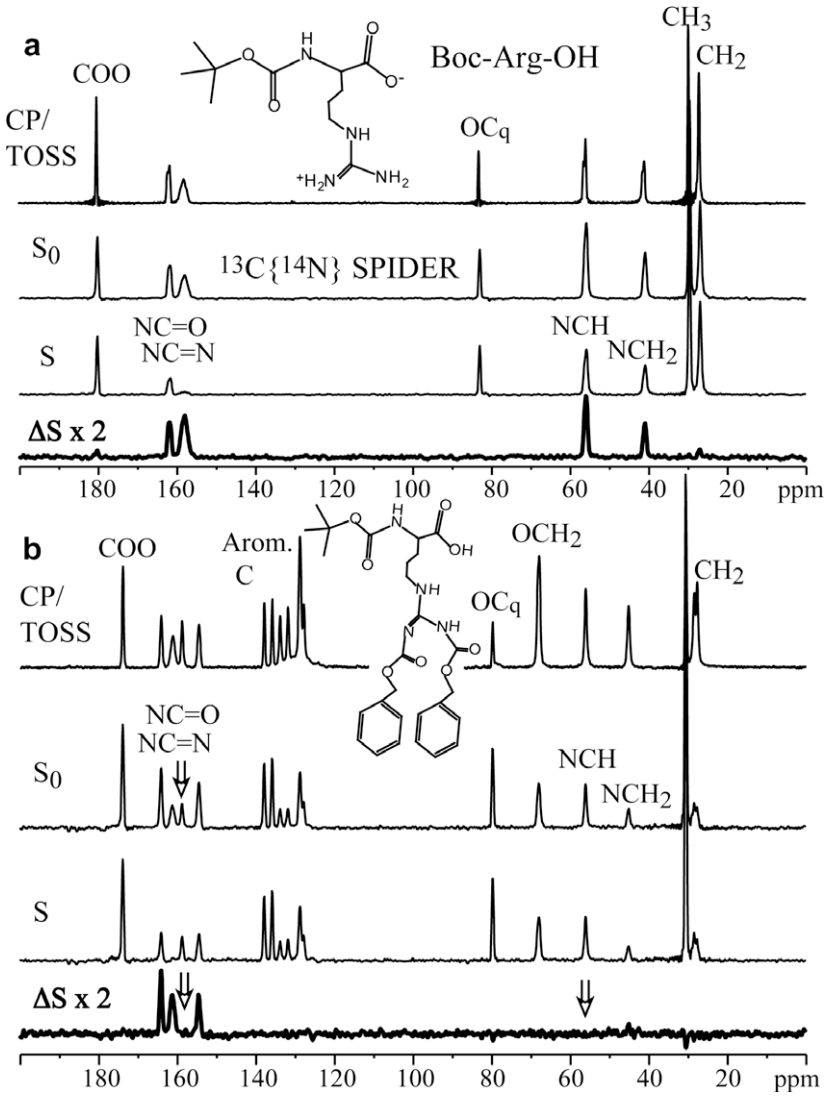


**Fig. 11.** CP/TOSS, $S_0$, S, and $\Delta S$ $^{13}C\{^{14}N\}$SPIDER spectra of (a) Boc—Arg—OH, which shows the expected dephasing; (b) Boc—Arg(Z)$_2$—OH, which shows $\Delta S = 0$ and low $S_0$ for two expected carbon signals, at 159 and 56 ppm (marked by arrows).

carbons is indicated in Fig. 14, which shows the dependence of $T_{2S,MAS}$ on $\omega_r$ for the non-protonated carbons. The curves show that the $T_{2S,MAS}$ values of the carbons bonded to N increase as spinning speed increases, most prominently for the 159-ppm carbon, which also showed the largest $\Delta S_0$ signal. At faster MAS, the rise of the curves becomes less obvious due to imperfect $^1$H decoupling resulting from interference by MAS. The measured data points are compared with simulated curves, and the fits give good estimates of the $^{14}$N $T_{1Q}$ relaxation times. The $^{14}$N bonded to the "backbone" carbon with a chemical shift of 159 ppm has a short $T_{1Q}$ relaxation time of ca. 0.2 ms, while the other $^{14}$N sites have $T_{1Q}$ values of ~2 ms. In the fit of the signal of the carbon resonating at 161 ppm, it was assumed that the three $^{14}$N to which it is bonded have the same $T_{1Q}$ of ~ 2 ms, giving an apparent $T_{1Q}^{app} = 0.67$ ms based on $1/T_{1Q}^{app} \approx 3 \times 1/(2\text{ ms})$.

### 3.4. Dynamics driving $T_{1Q}$-relaxation

The short $T_{1Q}$ of the nitrogen in the *N*-acetyl side groups of chitin is not too surprising, given that torsional fluctuations can rock the side group. In collagen and related peptides, motions of proline rings have been known to shorten $T_{1C}$ [23]. The mechanism of relaxation in Boc—Arg(Z)$_2$—OH is less obvious. In order to probe the MHz-rate motions that drive $T_{1Q}$ of $^{14}$N, we have measured the longitudinal $T_1$ relaxation times of all resolved carbon sites in Boc—Arg—OH and Boc—Arg(Z)$_2$—OH, see Fig. 15. The values show that the $T_{1C}$ values of sites near the —COOH group in the "backbone" of these two compounds are quite different, suggesting some changes around COOH in Boc—Arg(Z)$_2$—OH.

It is instructive to compare the measured $^{13}$C and estimated $^{14}$N $T_1$ relaxation times for neighboring sites. An approximate relationship can be obtained based on the following assumptions, which enable quantitative calculations [24]: (i) Dipolar interaction between $^{13}$C and $^1$H is the main spin-lattice relaxation mechanism for $^{13}$C. (ii) Quadrupolar coupling provides the dominant relaxation mechanism for $^{14}$N. (iii) The reorientational correlation times $\tau_c$ are identical for both $^{13}$C and $^{14}$N. (iv) The molecule undergoes isotropic motions. In the fast-motion limit, the relaxation rate of $^{13}$C due to C—H dipolar coupling can be given as:

$$1/T_{1C} = (4/3)\gamma_{13C}^2\gamma_{14N}^2\hbar S(S+1)r_{C-H}^{-6}\tau_c \quad (17)$$

and the quadrupolar relaxation rate of $^{14}$N is

$$1/T_{1Q} = (3/8)(e^2qQ/\hbar)^2\tau_c \quad (18)$$

With $r_{C-H} = 1.09$ Å and $e^2qQ/\hbar = 3$ MHz, we find

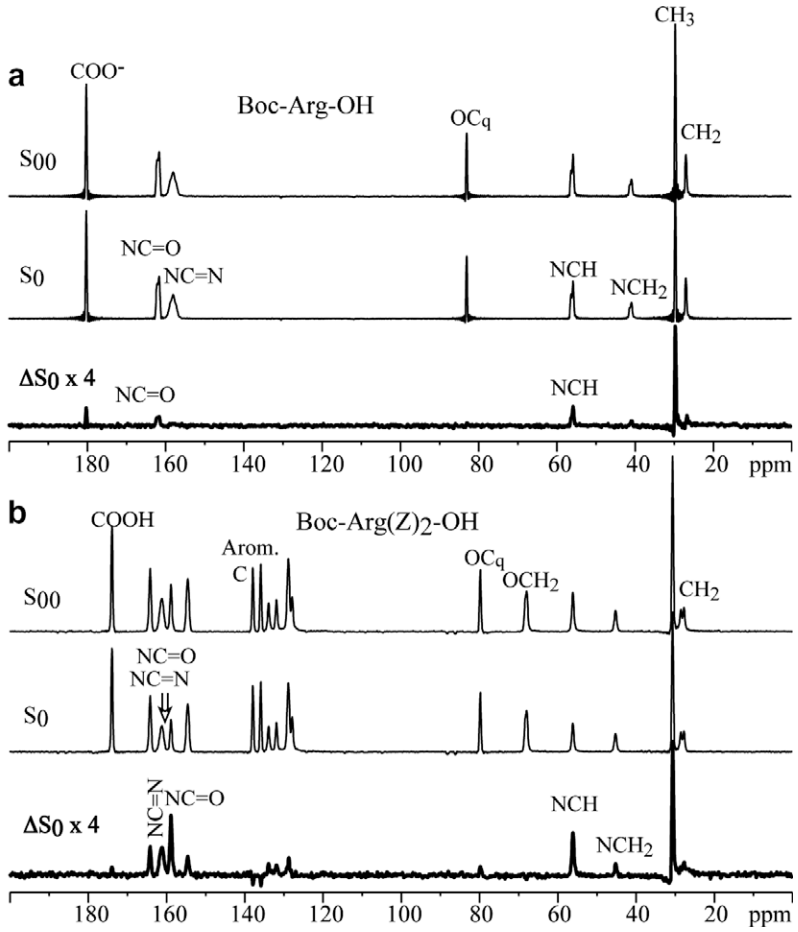


**Fig. 12.** $S_{00}$, $S_0$, and $\Delta S_0$ $^{13}$C spectra of (a) Boc—Arg—OH and (b) Boc—Arg(Z)$_2$—OH, which shows the largest $\Delta S_0 = S_{00} - S_0$ for the two carbon signals at 159 and 56 ppm.

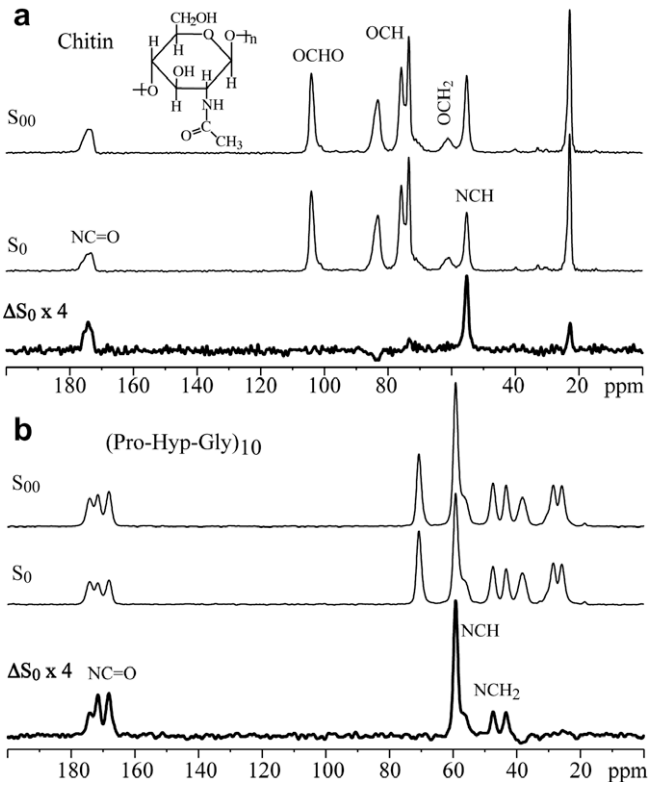


**Fig. 13.** $S_{00}$, $S_0$, and $\Delta S_0$ $^{13}$C spectra of (a) chitin and (b) $(POG)_{10}$. Significant $\Delta S_0$ signal is observed for all C bonded to N.

$$T_{1C} = 6200 T_{1Q} \quad (19)$$

From the experimentally measured $T_{1C}$ value of 11 s for $C_\alpha$ in N-t-Boc—Arg(Z)$_2$—OH, Eq. (19) yields an estimated $^{14}$N $T_{1Q}$ of 1.8 ms, within an order of magnitude from the 0.2-ms $T_{1Q}$ value estimated from $S_0$ and $T_{2S,MAS}$ data.

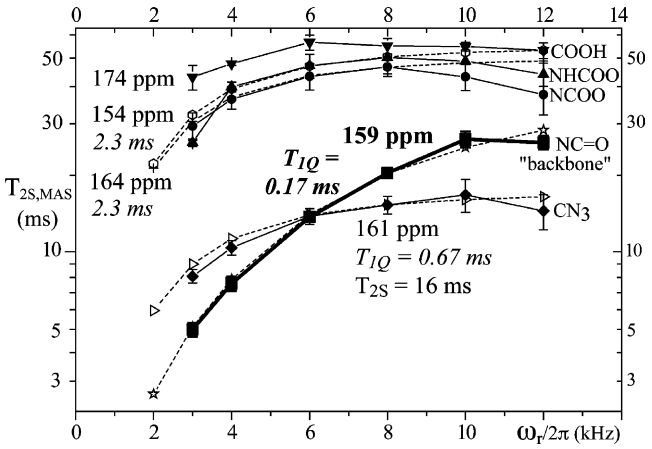


**Fig. 14.** Measurement of $T_{2C,MAS}$ as a function of spinning-frequency $\omega_r$ for various non-protonated $^{13}$C sites in Boc—Arg(Z)$_2$—OH. The fit curves (dashed lines and open symbols) are simulated with different values of $T_{1Q}$ and $T_2$: 159 ppm ($T_{1Q}$ = 0.17 ms, $T_2$ = 38 ms), 161 ppm (0.67 ms, 16 ms), 164 ppm (2.3 ms, 45 ms), 154 ppm (2.3 ms, 49 ms). The discrepancies between the measured and fit curves at $\omega_r/2\pi > 10$ kHz are due to imperfect $^1$H decoupling resulting from interference by fast spinning. The literature value of the C—N bond length in OCNH is 0.1339 nm, corresponding to $\delta_{SL} = 2\pi$ 1.8 kHz, which was used in these simulations.

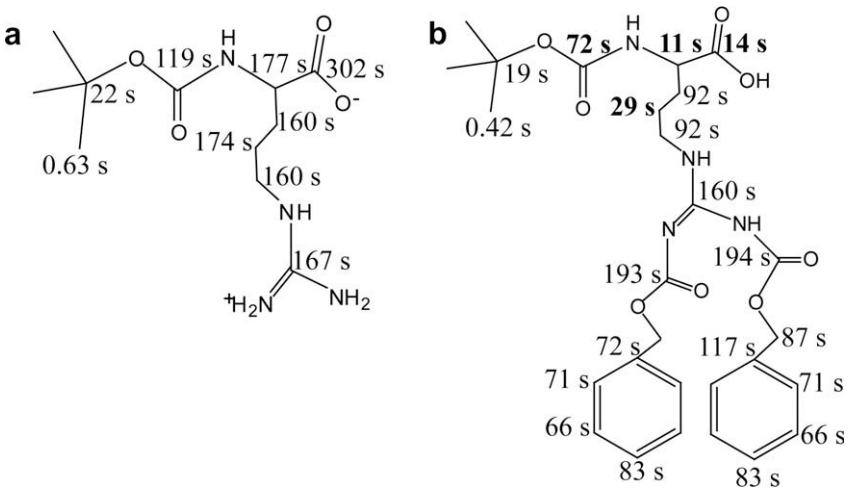


**Fig. 15.** Measured $T_{1C}$ relaxation times in (a) Boc—Arg—OH and (b) Boc—Arg(Z)$_2$—OH. Significantly shortened $T_{1C}$ values in Boc—Arg(Z)$_2$—OH are highlighted in bold.

In order to check for fast large-amplitude motions, the CSA powder patterns of the C=O carbons were measured by SUPER [25] experiments in both Boc—Arg—OH and Boc—Arg(Z)$_2$—OH. The powder patterns for the CO sites in Fig. 16 do not exhibit evidence of large-amplitude motions. The chemical shift anisotropies determined from these spectra are summarized in Table 2. Comparison with literature CSA data of carboxyl groups [26] suggests that the —COO group in Boc—Arg(Z)$_2$—OH is protonated, while that in Boc—Arg—OH is deprotonated. We suspect that the NH proton in the "backbone" undergoes some motion, since we only observed two protonated N in the $^{15}$N spectrum (not shown), while there are three protonated sites in the structure of Boc—Arg(Z)$_2$—OH. It is interesting to note that investigations of solid state proton exchange in a variety of organic compounds have also suggested that fast quadrupolar relaxation of $^{14}$N is induced by fluctuations in its electric field gradient that accompany proton exchange [27].

### 3.5. $T_{1Q}$ effects in J-coupled systems

This paper has focused on effects of $T_{1Q}$ relaxation of the heteronucleus under dipolar recoupling and under free MAS. As briefly indicated above, the effect analogous to that with dipolar recoupling occurs during "free MAS" under the influence of a heteronu-

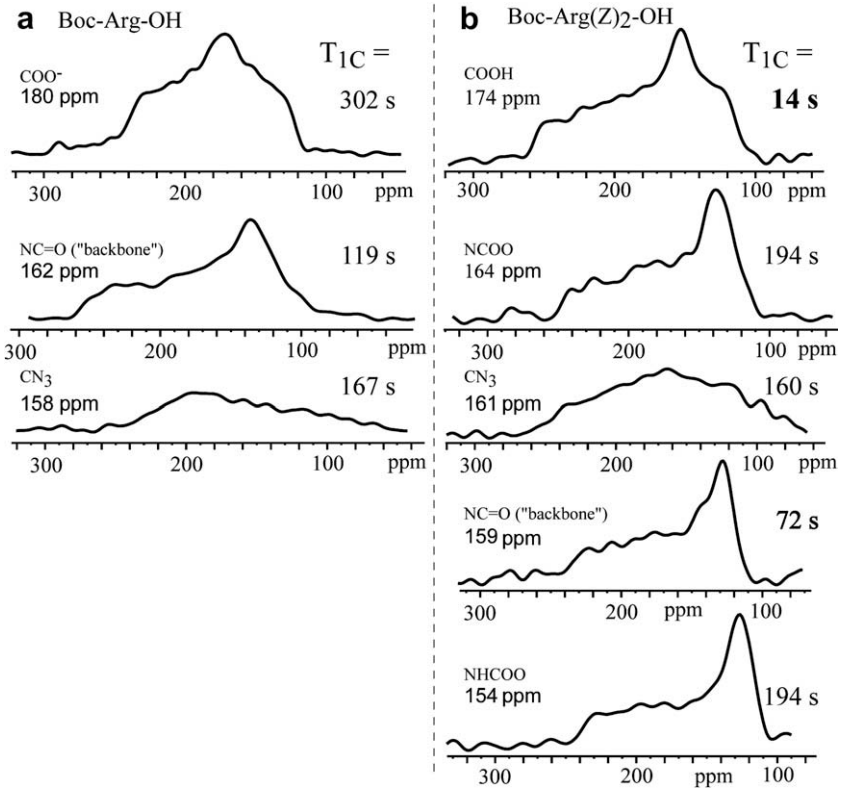


**Fig. 16.** COO powder patterns obtained as cross sections from 2D SUPER spectra of (a) Boc—Arg—OH and (b) Boc—Arg(Z)$_2$—OH. The $T_{1C}$ relaxation time of each site is listed to the right of its powder pattern.

**Table 2**
Summary of $^{13}C$ chemical shift principal values obtained from SUPER spectra of Boc—Arg—OH (compound 1) and Boc—Arg(Z)$_2$—OH (compound 2), and isotropic chemical shifts from MAS. Principal values have error margins of ±5 ppm.

| Compound | Carbon site | Chemical shift components(ppm) | | | $\Delta\sigma$ | $\sigma_{iso}$ |
|---|---|---|---|---|---|---|
| 1 | $COO^-$ | 242 | 174 | 124 | 118 | 180 |
| 2 | COOH | 257 | 153 | 113 | 144 | 174 |
| 1 | NC=O | 245 | 130 | 112 | 133 | 162 |
| 2 | NC=O | 232 | 125 | 125 | 107 | 159 |
| 2 | NHCOO | 234 | 115 | 115 | 119 | 154 |
| 2 | NCOO | 242 | 127 | 123 | 119 | 164 |

clear *J*-coupling [8]. In this case, the simulations for *S* dephasing with a single coupling frequency $\omega_{SL}$ (see Figs. 3a and S1a) are applicable. The $S_0$ experiment corresponds exactly to a Hahn-echo measurement of $T_2$, where the sign of the heteronuclear *J*-coupling is effectively inverted by a 180° pulse at $\tau = Nt_r/2$. Thus, the single-$\omega_{SL}$ $S_0$ decay curves as shown in Figs. 3b and S1b, including some slight oscillations, are expected to be observed in $T_2$ measurements of an *S*-nucleus *J*-coupled to a quadrupolar *L*-nucleus with short $T_{1Q}$.

In practice, *J*-couplings in the 1-kHz range are common for atoms with many electrons, i.e. for nuclides of higher mass. These have weak heteronuclear dipolar couplings due to the relatively large internuclear distances resulting from large atomic radii, but relatively large *J*-couplings. In $^{125}Te$ (S = 1/2) NMR of $Sb_2Te_3$, we have indeed observed shortened $T_{2,Te,MAS} \approx 0.4$ ms compared to Te in PbTe or GeTe, together with a short $T_{1Q,Sb,MAS} \approx 0.5$ ms for the central transition of $^{121}Sb$ ($L = 5/2$).

### 3.6. Unpaired electrons

The dipolar coupling of nuclear spins with unpaired electrons of short longitudinal relaxation time or fast longitudinal spin exchange is another case where multi-spin coherence is generated by a coupling, decays fast due to relaxation or spin exchange of the (electron) *L*-spin, and shortens the $T_{2,\,MAS}$ of the observed nucleus *S*. The quantitative analysis of this effect, where the couplings can be much larger than considered here (>$\omega_r$, while we implicitly assumed $\omega_{SL} < \omega_r$) and must be described by more complex interactions [28] is beyond the scope of this article.

## 4. Conclusions

The effects of fast longitudinal relaxation of a quadrupolar nucleus coupled to the observed spin-1/2 nucleus have been studied theoretically and experimentally. Theoretical analysis and simulations have shown that short $T_{1Q}$ can cause significant reduction or even disappearance of $\Delta S$ signals in experiments like REDOR and SPIDER. In order to demonstrate and minimize the effect, a new pulse sequence with minimal recoupling has been designed and shown to produce an improved reference signal $S_{00}$. A significant difference signal $\Delta S_0 = S_{00} - S_0$ proves coupling to a heteronucleus with $T_{1Q} \sim 0.3$ ms. Applications to a molecular crystal, to an *N*-acetylated polysaccharide, and to a collagen-mimetic oligopeptide show that the effect is quite common. Furthermore, studies of $T_{1Q}$-enhanced, $\omega_r$-dependent $T_{2S,MAS}$ relaxation under free MAS without recoupling have shown both theoretically and experimentally that short $T_{1Q}$ (5–200 μs) of the coupled heteronucleus can cause a strong decrease in the apparent $T_{2S,MAS}$ of the observed nucleus; fast spinning helps greatly to lengthen $T_{2S,\,MAS}$. Simulations of the spinning-speed dependence provide good estimates of $T_{1Q}$. Finally, possible reasons for the short $T_{1Q}$ values of $^{14}N$ in the studied compounds have been explored.

## 5. Experimental

### 5.1. Samples

Arginine derivatives, $N_\alpha$-(*tert*-butoxycarbonyl)-L-arginine (Boc—Arg—OH) and $N_\alpha$-Boc-$N_\delta$, $N_\omega$-di-Z-L-arginine (Boc—Arg(Z)$_2$—OH), were obtained from Sigma–Aldrich. Boc—Arg(Z)$_2$—OH was 98% pure, and Boc—Arg—OH contained 5–10% *n*-butanol. Chitin (poly (*N*-acetyl-1, 4-β-D-glucopyranosamine) was purchased from Fluka. $(POG)_{10}$ was purchased from Peptide Institute, Japan. All samples were used without further treatment.

### 5.2. NMR parameters

The NMR experiments were performed using a Bruker DSX400 spectrometer at 400 MHz for $^1H$, 100 MHz for $^{13}C$, and 29 MHz for $^{14}N$. A Bruker 4-mm triple-resonance probe head was used for the SPIDER experiments at a 5-kHz spinning-frequency, with ca. 56 kHz $^1H$ decoupling power, which is increased to 63 kHz during $^{13}C$ $\pi$ pulses. The $^{14}N$ radio-frequency field strength was $\gamma_N B_1 \approx 2\pi$ 30 kHz, and the $^{13}C$ 180° pulse length was 8.1 μs. The recoupled dipolar evolution consisted of eight rotation periods (1.6 ms), and the $^{14}N$ irradiation time of four rotation periods. The 5-kHz MAS experiments using the pulse sequences shown in Fig. 8a and b for measuring the regular and an improved reference signal $S_0$ and $S_{00}$, respectively, and $\Delta S_0$ were performed with a 4-mm probe head in double-resonance mode. All experiments were performed with a cross polarization (CP) contact time of 1 ms and a recycle delay of 2 s. In measurements of $S_0$ and $S_{00}$, the $^{13}C$ irradiation frequency "on-resonance" was set near protonated carbon resonances during the $^{13}C$ 180° pulse train and near those of non-protonated carbon resonances during detection. The gated decoupling time before detection in measuring $S_{00}$ was 6 μs.

SUPER experiments were used to obtain $^{13}C$ CSA powder patterns in the arginine derivatives. These experiments were carried out at a spinning speed of 5 kHz. The $^{13}C$ field strength of the 360° pulses was 62.5 kHz and the number of $t_1$ increments was 96, with an acquisition time of 5 ms.

$T_1$ and $T_2$ relaxation time measurements were made after 1-ms cross polarization time, using a z-filter and Hahn-echo, respectively. TOSS was used before and TPPM $^1H$ decoupling during detection.

## Acknowledgments

This work was supported by the U.S. Department of Energy – Basic Energy Sciences under Contract No. DE-AC02-07CH11358. We thank M. Hong and Y. Zhang for making the $(POG)_{10}$ sample available.

## Appendix A. Free heteronuclear evolution with $T_{1Q}$ relaxation, and numerical calculation

Heteronuclear evolution with longitudinal *L*-spin relaxation is governed by the von Neumann equation with relaxation, $d\rho/dt = -i/\hbar[H_{SL},\rho] + \underline{R}\,\rho$, Eq. (6), where the Redfield supermatrix $\underline{R}$ acts only on the *L*-spin part of the density matrix; its effect is given by the relaxation exchange matrix W according to Eq. (2). Inserting the density matrix for $L = 1$, $\rho(t) = S_x\ \mathrm{diag}(p_{x,1},\ p_{x,0},\ p_{x,-1}) + S_y\ \mathrm{diag}$ $(p_{y,1},\ p_{y,0},\ p_{y,-1})$, into Eq. (6) gives

$$\begin{aligned} d\rho/dt = S_y\{&\omega_{SL}\mathrm{diag}(p_{x,1},0,-p_{x,-1}) + \mathrm{diag}(\underline{W}(p_{y,1},p_{y,0},p_{y,-1}))\} \\ &+ S_x\{-\omega_{SL}\mathrm{diag}(p_{y,1},0,-p_{y,-1}) + \mathrm{diag}(\underline{W}(p_{x,1},p_{x,0},p_{x,-1}))\} \end{aligned} \quad (A1)$$

This can be set equal to the standard expression for the time derivative of $\rho(t)$,

$$\begin{aligned} d\rho/dt &= S_x \mathrm{diag}(dp_{x,1}/dt, dp_{x,0}/dt, dp_{x,-1}/dt) \\ &+ S_y \mathrm{diag}(dp_{y,1}/dt, dp_{y,0}/dt, dp_{y,-1}/dt) \end{aligned} \tag{A2}$$

Generalizing to arbitrary $L$-spin, Eqs. (A1) and (A2) can be used to generate $2(2L+1)$ coupled differential equations for the $p$-coefficients:

$$\begin{aligned} dp_{y,m}/dt &= \omega_{SL} m p_{x,m} + \sum_{m'} W_{mm'} p_{y,m'} \\ dp_{x,m}/dt &= -\omega_{SL} m p_{y,m} + \sum_{m'} W_{mm'} p_{x,m'} \end{aligned} \tag{A3}$$

which are equivalent to Eq. (59) in Ref. [29]. In the absence of relaxation ($\underline{W} = 0$), the solutions are the well-known sinusoidal oscillations, but with relaxation the solutions are much more complicated.

For $L = 1/2$, the four coupled Eq. (A3) can be solved analytically, as shown in Appendix B. For $L > 1/2$, it is more convenient to evaluate $\Delta p = dp/dt\ \Delta t$ numerically time-step by time-step, using

$$\begin{aligned} \mathbf{r}_y &= \underline{W}(p_{y,L}, p_{y,(L-1)}, \ldots, p_{y,-(L-1)}, p_{y,-L}) \\ \mathbf{r}_x &= \underline{W}(p_{x,L}, p_{x,(L-1)}, \ldots, p_{x,-(L-1)}, p_{x,-L}) \\ \Delta p_{y,m} &= \{\omega_{SL} m p_{x,m} + r_{y,m}\}\Delta t \\ \Delta p_{x,m} &= \{-\omega_{SL} m p_{y,m} + r_{y,m}\}\Delta t \\ p_{y,m}(t+\Delta t) &= p_{y,m}(t) + \Delta p_{y,m} \\ p_{x,m}(t+\Delta t) &= p_{x,m}(t) + \Delta p_{x,m} \end{aligned} \tag{A4}$$

A time step of $\Delta t = 0.1$ μs was shown to produce the same results as shorter steps and was used in all the numerical simulations. Alternatively, one can use Abragam's exponential-matrix solutions [29].

## Appendix B. Analytical REDOR signal for $L = 1/2$

For $L = 1/2$, Eq. (A3) gives four coupled equations,

$$dp_{y,+1/2}/dt = \omega_{SL} 1/2 p_{x,+1/2} - r(p_{y,+1/2} - p_{y,-1/2}) \tag{B1a}$$
$$dp_{y,-1/2}/dt = \omega_{SL}(-1/2) p_{x,-1/2} + r(p_{y,+1/2} - p_{y,-1/2}) \tag{B1b}$$
$$dp_{x,+1/2}/dt = -\omega_{SL} 1/2 p_{y,+1/2} - r(p_{x,+1/2} - p_{x,-1/2}) \tag{B1c}$$
$$dp_{x,-1/2}/dt = -\omega_{SL}(-1/2 p_{y,-1/2}) + r(p_{x,+1/2} - p_{x,-1/2}) \tag{B1d}$$

with $r = 1/(2T_{1L})$. Given that $p_{x,-1/2}(0) = p_{x,+1/2}(0)$ and $p_{y,-1/2}(0) = -p_{y,+1/2}(0)$, we can set $p_{x,-1/2} = p_{x,+1/2} = p_x$ and $p_{y,-1/2} = -p_{y,+1/2} = -p_y$. This makes Eqs. (B1b) and (B1d) redundant, leaving

$$dp_y/dt = p_x \omega_{SL}/2 - p_y 2r \tag{B2a}$$
$$dp_x/dt = p_y(-\omega_{SL})/2 \tag{B2b}$$

Here, it is straightforward to incorporate transverse $T_{2S}$ relaxation of the $S$-spin:

$$dp_y/dt = p_x \omega_{SL}/2 - p_y(1/T_{2S} + 1/T_{1L}) \tag{B3a}$$
$$dp_x/dt = p_y(-\omega_{SL})/2 - p_x/T_{2S} \tag{B3b}$$

The factor of 1/2 in front of $\omega_{SL}$ is usually avoided in calculations limited to spin-1/2 by writing a factor of 2 in front of the right-hand side of the Hamiltonian in Eq. (7), but this is not advisable in calculations for general $L$ that are also of interest here. The solutions for the initial condition $p_x = 1$, $p_y = 0$ differ qualitatively whether

$$w = \sqrt{\omega_{SL}^2 T_{1L}^2 - 1} \tag{B4}$$

is real or imaginary:

For long $T_{1L} > 1/\omega_{SL}$, $w$ is real, and we obtain oscillatory solutions

$$p_x(t, T_{1L}) = e^{-\left(\frac{1}{2T_{1L}} + \frac{1}{T_{2S}}\right)t}\left(\cos\frac{wt}{2T_{1L}} + \frac{1}{w}\sin\frac{wt}{2T_{1L}}\right) \tag{B5a}$$

$$p_y(t, T_{1L}) = \frac{1}{w} e^{-\left(\frac{1}{2T_{1L}} + \frac{1}{T_{2S}}\right)t}\left(\sin\frac{wt}{2T_{1L}}\right) T_{SL}\omega_{SL} \tag{B5b}$$

For short $T_{1L} < 1/\omega_{SL}$, $w$ is imaginary, and we obtain

$$p_x(t, T_{1L}) = e^{-\left(\frac{1}{2T_{1L}} + \frac{1}{T_{2S}}\right)t}\left(\cosh\frac{|w|t}{2T_{1L}} + \frac{1}{|w|}\sinh\frac{|w|t}{2T_{1L}}\right) \tag{B5c}$$

$$p_y(t, T_{1L}) = \frac{1}{|w|} e^{-\left(\frac{1}{2T_{1L}} + \frac{1}{T_{2S}}\right)t}\left(\sinh\frac{|w|t}{2T_{1L}}\right) T_{SL}\omega_{SL} \tag{B5d}$$

Note that in recoupling experiments, $t$ is usually denoted as $Nt_r$. Curves calculated based on Eqs. (B5a) and (B5c) are shown in Fig. 2a.

The reference signal $S_0$ is obtained by applying one more or one less inversion pulse at the center of the recoupling period. This is equivalent to an inversion of the effective heteronuclear coupling frequency $\omega_{SL}$ in Eq. (B2) at $Nt_r/2$. The solutions in Appendix B can be used to calculate the initial condition for the second part of the heteronuclear evolution, i.e. $p_x^0(0) = p_x(Nt_r/2)$ and $p_y^0(0) = p_y(Nt_r/2)$ with $p_x$ and $p_y$ as given in Eq. (B5).

For long $T_{1L} > 1/\omega_{SL}$, $w$ is real, and

$$p_x^0(t, T_{1L}) = e^{-\left(\frac{1}{2T_{1L}} + \frac{1}{T_{2S}}\right)t}\left(-\frac{1}{w^2}\cos\frac{wt}{2T_{1L}} + \frac{1}{w}\sin\frac{wt}{2T_{1L}} - \frac{\omega_{SL}^2 T_{1L}^2}{w^2}\right) \tag{B6a}$$

For short $T_{1L} < 1/\omega_{SL}$, $w$ is imaginary, and

$$p_x^0(t, T_{1L}) = e^{-\left(\frac{1}{2T_{1L}} + \frac{1}{T_{2S}}\right)t}\left(-\frac{1}{w^2}\cosh\frac{|w|t}{2T_{1L}} + \frac{1}{|w|}\sinh\frac{|w|t}{2T_{1L}} - \frac{\omega_{SL}^2 T_{1L}^2}{w^2}\right) \tag{B6b}$$

For all $T_{1L}$ values,

$$p_y^0(t, T_{1Q}) = \left(1 - \frac{1}{w^2}\right) e^{-\left(\frac{1}{2T_{1L}} + \frac{1}{T_{2S}}\right)t}\left(1 - e^{-\frac{wt}{2T_{1L}}}\right) \tag{B6c}$$

Curves calculated from Eqs. (B6a) and (B6b) are shown in Fig. 2b.

## Appendix C. $T_{1Q}$-dependence of the REDOR decay constant $T_{SL}$

From numerical REDOR simulation for spin $L = 1$ with $T_{1Q}$ relaxation of the $L$-spin, we have determined the dependence of the time constant $T_{SL}$ in REDOR $S$ and $S_0$ experiments on $T_{1Q}$, see Fig. 4. Some aspects of these $T_{SL}$ vs. $T_{1Q}$ curves were difficult to explain quantitatively based on a qualitative analysis. In the following, we derive these features based on the analytical analysis for $L = 1/2$. For all cases, we assume that $T_{2S} \gg T_{1L}$, so that the effect of $T_{1L}$ is not masked by fast $T_{2S}$ decay. Analytical simulations of $T_{SL}$ vs. $T_{1L}$ for spin $L = 1/2$ are plotted in Fig. S2 (see Supporting material); they closely resemble the numerical results for $L = 1$ shown in Fig. 4.

For short $T_{1L} \ll 1/\omega_{SL}$, $|w| \sim 1$, and Eq. (B5c) for the dephased signal $S$ can be approximated as

$$p_x(t, T_{1L}) \approx e^{-\left(\frac{1-|w|}{2T_{1L}}\right)t} \tag{C1a}$$

so the decay constant is

$$T_{SL} = \frac{2T_{1L}}{1-|w|} \approx \frac{2T_{1L}}{\frac{1}{2}(2T_{1L})^2\left(\frac{\omega_{SL}}{2}\right)^2} = \frac{4}{\omega_{SL}^2 T_{1L}} \tag{C1b}$$

which gives Eq. (11).

For long $T_{1L} \gg 1/\omega_{SL}$, we have $w \sim T_{1L}\omega_{SL}$ and Eq. (B5a) can be simplified to

$$p_x(t, T_{1L}) \approx e^{-\frac{t}{2T_{1L}}}\left(\cos\frac{\omega_{SL} t}{2}\right) \tag{C2a}$$

where the decay is due to the $\cos(\omega_{SL}t/2)$ oscillation and therefore independent of $T_{1L}$; this corresponds to the long-time plateaus in the $T_{SL}$ vs. $T_{1L}$ curves for REDOR $S$ in Fig. S2.

The REDOR reference signal $S_0$ of Eq. (B6b) can be simplified for short $T_{1L} \ll 1/\omega_{SL}$, where $|w| \sim 1$:

$$p_x^0(t, T_{1L}) = e^{-\frac{1}{2T_{1L}}t}\left(\cosh\frac{|w|t}{2T_{1L}} + \sinh\frac{|w|t}{2T_{1L}}\right) = e^{-\frac{1}{2T_{1L}}t}e^{\frac{|w|}{2T_{1L}}t}$$
$$= e^{-\frac{(1-|w|)}{2T_{1L}}t} \approx p_x(t, T_{1L}) \quad \text{(C3a)}$$

In other words, $S_0 \approx S$, which explains the overlap of the curves for $S$ and $S_0$ in Fig. S2 for short $T_{1Q}$ values.

For long $T_{1L} \gg 1/\omega_{SL}$, $w \sim T_{1L}\omega_{SL}$, and

$$p_x^0(t, T_{1L}) = e^{-\frac{t}{2T_{1L}}}(0 + 0 - (-1)) = e^{-\frac{t}{2T_{1L}}} \quad \text{(C3b)}$$

which gives $T_{SL} \sim 2T_{1L}$ independent of $\omega_{SL}$, as observed in Fig. S2.

## Appendix D. Supplementary data

Supplementary data associated with this article can be found, in the online version, at doi:10.1016/j.jmr.2008.12.021.

## References


[1] T. Gullion, A.J. Vega, Measuring heteronuclear dipolar couplings for I = 1/2, S > 1/2 spin pairs by REDOR and REAPDOR NMR, Progr. Nucl. Magn. Reson. Spectrosc. 47 (2005) 123–136.

[2] I. Schnell, Dipolar recoupling in fast-MAS solid-state NMR spectroscopy, Progr. Nucl. Magn. Reson. Spectrosc. 45 (2004) 145–207.

[3] T. Gullion, Detecting $^{13}C$–$^{17}O$ dipolar interactions by rotational-echo, adiabatic-passage, double-resonance NMR, J. Magn. Reson. 117 (1995) 326–329.

[4] E. Hughes, T. Gullion, A. Goldbourt, S. Vega, A.J. Vega, Internuclear distance determination of S = 1, I = 1/2 spin pairs using REAPDOR NMR, J. Magn. Reson. 156 (2002) 230–241.

[5] K. Schmidt-Rohr, J.D. Mao, Selective observation of nitrogen-bonded carbons in solid-state NMR by saturation-pulse induced dipolar exchange with recoupling, Chem. Phys. Lett. 359 (2002) 403–441.

[6] S. Cavadini, A. Abraham, G. Bodenhausen, Coherence transfer between spy nuclei and nitrogen-14 in solids, J. Magn. Reson. 190 (2008) 160–164.

[7] Z. Gan, $^{13}C/^{14}N$ heteronuclear multiple-quantum correlation with rotary resonance and REDOR dipolar recoupling, J. Magn. Reson. 184 (2007) 39–43.

[8] A. Abragam, Principles of Nuclear Magnetism, Ch. XI, Sect. III, Clarendon Press, Oxford, 1983.

[9] C.-G. Hoelger, E. Roessler, B. Wehrle, F. Aguilar-Parrilla, H.-H. Limbach, Self-decoupling of $^{15}N$–$^{14}N$ dipole-quadrupole couplings in $^{15}N$ CPMAS NMR spectra and molecular motions in crystalline hydrazine sulfate, *p*-(diethylamino)benzaldehyde diphenylhydrazone, and its solid solution in polycarbonate, J. Phys. Chem. 99 (1995) 14271–14276.

[10] R.W. Schurko, R.E. Wasylishen, J.H. Nelson, Effect of cobalt-59 self-decoupling on the solid-state $^{31}P$ CP/MAS NMR spectra of cobaloximes, J. Phys. Chem. 100 (1996) 8057–8060.

[11] R.K. Harris, A.C. Olivieri, Quadrupolar effects transferred to spin-1/2 magic-angle spinning spectra of solids, Progr. Nucl. Magn. Reson. Spectrosc. 24 (1992) 435–456.

[12] A. Naito, P.B. Barker, C.A. McDowell, Two-dimensional nuclear magnetic resonance studies on a single crystal of l-alanine. Separation of the local dipolar fields; and 2D exchange spectroscopy of the nitrogen-14 relaxation processes, J. Chem. Phys. 81 (1984) 1583–1591.

[13] K. Saalwachter, K. Schmidt-Rohr, Relaxation-induced dipolar exchange with recoupling — an MAS NMR method for determining heteronuclear distances without irradiating the second spin, J. Magn. Reson. 145 (2000) 161–172.

[14] A. Suter, M. Mali, J. Roos, D. Brinkmann, Mixed magnetic and quadrupolar relaxation in the presence of a dominant static Zeeman Hamiltonian, J. Phys. Condens. Mater. 10 (1998) 5977–5994.

[15] J.P. Yesinowski, Magnetization-recovery experiments for static and MAS-NMR of I = 3/2 nuclei, J. Magn. Reson. 180 (2006) 147–161.

[16] H.W. Spiess, Deuteron spin alignment: a probe for studying ultraslow motions in solids and solid polymers, J. Chem. Phys. 72 (1980) 6755–6762.

[17] A.E. McDermott, F. Creuzet, R. Gebhard, K. van der Hoef, M.H. Levitt, J. Herzfeld, J. Lugtenburg, R.G. Griffin, Determination of internuclear distances and the orientation of functional groups by solid-state NMR: rotational resonance study of the conformation of retinal in bacteriorhodopsin, Biochemistry 33 (1994) 6129–6136.

[18] M. Ernst, A. Verhoeven, B.H. Meier, High-speed magic-angle spinning $^{13}C$ MAS NMR spectra of adamantane: self-decoupling of the heteronuclear scalar interaction and proton spin diffusion, J. Magn. Reson. 130 (1998) 176–185.

[19] B.H. Meier, Polarization transfer and spin diffusion in solid-state NMR, Adv. Magn. Opt. Reson. 18 (1994) 1–116.

[20] M. Bak, J.T. Rasmussen, N.C. Nielsen, SIMPSON. A general simulation program for solid-state NMR spectroscopy, J. Magn. Reson. 147 (2000) 296–330.

[21] A.J. Shaka, J. Keeler, M.B. Smith, R. Freeman, Spatial localization of NMR signals in an inhomogeneous radiofrequency field, J. Magn. Reson. 61 (1985) 175–180.

[22] K. Schmidt-Rohr, H.W. Spiess, Multidimensional Solid-State NMR and Polymers, Academic Press, San Diego, 1994.

[23] S.K. Sarkar, P.E. Young, C.E. Sullivan, D.A. Torchia, Proline ring motion in solid state: a deuterium NMR study, Pept. Struct. Funct. Proc. Am. Pept. Symp. 9 (1985) 121–124.

[24] H.W. Spiess, Rotation of molecules and nuclear spin relaxation, Nucl. Magn. Reson. 15 (1978) 55.

[25] S.F. Liu, J.D. Mao, K. Schmidt-Rohr, A robust technique for two-dimensional separation of undistorted chemical-shift anisotropy powder patterns in magic-angle-spinning NMR, J. Magn. Reson. 155 (2002) 15–28.

[26] Z. Gu, D.G. Drueckhammer, L. Kurz, K. Liu, D.P. Martin, A. McDermott, Solid state NMR studies of hydrogen bonding in a citrate synthase inhibitor complex, Biochemistry 38 (1999) 8022–8031.

[27] S.H. Alarcon, A.C. Olivieri, P. Jonsen, Carbon-13 CPMAS NMR study of solid arylazonaphthols. Evidence of carbon-13, nitrogen-14 self-decoupling induced by a solid-state proton transfer reaction, Perkin Trans. 2 (1993) 1783–1786.

[28] A. Nayeem, J.P. Yesinowski, Calculation of magic-angle spinning nuclear magnetic resonance spectra of paramagnetic solids, J. Chem. Phys. 89 (1988) 4600–4608.

[29] A. Abragam, Principles of Nuclear Magnetism, Ch. X, Sect. IV, Clarendon Press, Oxford, 1983.